When H II regions are complicated

considering perturbations from winds, radiation pressure, and other effects

Geen, S.; Pellegrini, E.; Bieri, R.; Klessen, R.

DOI
10.1093/mnras/stz3491

Publication date
2020

Document Version
Final published version

Published in
Monthly Notices of the Royal Astronomical Society

Monthly Notices
of the
ROYAL ASTRONOMICAL SOCIETY

MNRAS **492,** 915–933 (2020)
Advance Access publication 2019 December 11

doi:10.1093/mnras/stz3491

When H II regions are complicated: considering perturbations from winds, radiation pressure, and other effects

Sam Geen [1,2]★ Eric Pellegrini,[1] Rebekka Bieri[3] and Ralf Klessen[1,4]

[1]*Zentrum für Astronomie, Institut für Theoretische Astrophysik, Universität Heidelberg, Albert-Ueberle-Str 2, D-69120 Heidelberg, Germany*
[2]*Anton Pannekoek Institute for Astronomy, Universiteit van Amsterdam, Science Park 904, NL-1098 XH Amsterdam, the Netherlands*
[3]*Max-Planck-Institute for Astrophysics, Karl-Schwartzschild-Strasse 1, Garching, 85748, Germany*
[4]*Interdisziplinäres Zentrum fur Wissenschaftliches Rechnen, Universität Heidelberg, INF 205, D-69120 Heidelberg, Germany*

Accepted 2019 December 9. Received 2019 December 9; in original form 2019 June 13

ABSTRACT

We explore to what extent simple algebraic models can be used to describe H II regions when winds, radiation pressure, gravity, and photon breakout are included. We (a) develop algebraic models to describe the expansion of photoionized H II regions under the influence of gravity and accretion in power-law density fields with $\rho \propto r^{-w}$, (b) determine when terms describing winds, radiation pressure, gravity, and photon breakout become significant enough to affect the dynamics of the H II region where $w = 2$, and (c) solve these expressions for a set of physically motivated conditions. We find that photoionization feedback from massive stars is the principal mode of feedback on molecular cloud scales, driving accelerating outflows from molecular clouds in cases where the peaked density structure around young massive stars is considered at radii between ∼0.1 and 10–100 pc. Under a large range of conditions the effect of winds and radiation on the dynamics of H II regions is around 10 per cent of the contribution from photoionization. The effect of winds and radiation pressure is most important at high densities, either close to the star or in very dense clouds such as those in the Central Molecular Zone of the Milky Way. Out to ∼0.1 pc they are the principal drivers of the H II region. Lower metallicities make the relative effect of photoionization even stronger as the ionized gas temperature is higher.

Key words: methods: analytical – stars: formation – stars: massive – ISM: clouds – H II regions.

1 INTRODUCTION

Massive stars produce large quantities of energy as radiation and kinetic outflows that shape astrophysical phenomena on a wide range of scales. For a holistic view of this process of stellar 'feedback', we must understand the behaviour of such flows on a systemic level. In this paper, we produce new models to describe the evolution of feedback structures around massive stars in their natal environment, H II regions. These are important in understanding how kinetic energy and radiation from massive stars are transmitted from the sub-parsec scale to the galactic scale.

H II regions are volumes of ionized hydrogen around massive stars. Their evolution is a complex process, affected by stellar evolution, gas dynamics, and the interaction of different feedback processes. The complexity of the problem creates a large parameter space to study.

Recently, numerical simulations have been used to model H II regions with increasing physical fidelity, but they are expensive and do not offer descriptive explanations for why a certain set of model assumptions leads to a particular outcome. Algebraic expressions that describe H II regions, while much simplified, allow faster parameter space exploration and quantitative predictions. A large body of analytic work exists to describe individual processes that shape H II regions, and to some extent how they interact, though this work is often limited in its predictive power by (necessary) simplifications made in describing the modelled systems (see references in Sections 1.1–1.4).

This work brings three new insights to the problem. First, we provide a new dynamical equation to describe the evolution of photoionized H II regions from young massive stars sitting inside physically motivated power-law gas density profiles ($\rho \propto r^{-w}$) with gravity and accretion. This equation behaves differently to previous formulations of the expansion in uniform environments.

Secondly, we provide formulations for how winds, radiation pressure, photon breakout, and self-gravity influence these H II regions when $w = 2$.

★ E-mail: sam.geen@uni-heidelberg.de

Thirdly, we calculate surfaces in phase space where winds, radiation pressure, gravity, and photon breakout significantly shape the evolution of H II regions in physically motivated conditions. With this, we seek to address the question of when H II regions are *complicated*, i.e. where we must use more detailed numerical solutions than our simple algebraic models to explain their evolution.

We begin this section by summarizing existing analytic work on the evolution of H II regions. We describe theory for how the photoionization of H to H^+ leads to an overpressurized, expanding structure. We then discuss theory of stellar winds and direct radiation pressure, and study how these processes interact with the photoionized H II region. Finally, we lay out the structure of this paper and how we address this problem.

1.1 Photoionized H II regions

The evolution of H II regions has been studied widely using observations, analytic theory, and more recently, hydrodynamical simulations. Theories governing their expansion have been proposed by several authors since the 1950s. Hydrogen is ionized by photons with energies above 13.6 eV, while dust and other species can be ionized by lower energy photons. Kahn (1954) derived plane-parallel equations to describe ionization fronts. They defined a transition between R-type fronts, where the front is bounded by the ability for new ionizing photons to reach neutral gas, and D-type fronts, which are in photoionization equilibrium and expand because they are warmer and therefore overpressured compare to the surrounding medium (approx. 10^4 K versus 10–100 K). In a uniform medium, the ionization front typically begins in the R-type phase and over approximately one recombination time (the amount of time it takes for the ionized gas to recombine to its neutral state) it transitions to the D-type phase. This time is typically short in dense cloud environments (see our previous analysis in Geen et al. 2015a).

Spherically symmetric solutions were derived by authors such as Spitzer (1978), Dyson & Williams (1980), and Franco, Tenorio-Tagle & Bodenheimer (1990), while Whitworth (1979) and Franco, Tenorio-Tagle & Bodenheimer (1989) describe 'blister' H II regions located close to the cloud surface and able to escape preferentially from the cloud in one direction. More recently, Hosokawa & Inutsuka (2006) and Raga, Canto & Rodriguez (2012) modified these equations to consider the inertia of the shell and external pressure terms from the neutral gas. These results have been used to test simulation codes by Bisbas et al. (2015) and in various more physically complete models.

On small scales, Keto (2002, 2007) model ultracompact H II regions whose expansion is resisted by the gravity of, and accretion on to, a massive protostar. Shapiro et al. (2006) describe relativistic ionization fronts in cosmological conditions, while Alvarez, Bromm & Shapiro (2006) derive a condition for H II regions to overflow the D-type front based on the solutions of Shu et al. (2002), which has been explored in nearby galaxies by Seon & Kwang-Il (2009) and Pellegrini et al. (2012). The solutions given in these papers were further extended and applied by Tremblin et al. (2014), Didelon et al. (2015), and Geen et al. (2015b) to describe the evolution of H II regions in observed and simulated molecular clouds, assuming different external density profiles. In Section 4, we use these model assumptions to derive a dynamical equation for how gravity and accretion shape H II regions in power-law density fields found around young massive stars in clumps and molecular clouds.

See the review by Dale (2015) or the introduction of Geen et al. (2018) for a more detailed discussion on 3D numerical simulations of photoionized H II regions, which are beyond the scope of this paper.

1.2 Stellar winds

Stellar winds ejected from the surface of the star directly deposit kinetic energy into the circumstellar medium. Early work by Avedisova (1972), Castor, Weaver & McCray (1975), and Weaver et al. (1977) demonstrated that in the absence of radiative cooling, the cumulative energy emitted by a star over its lifetime can drive the expansion of hot bubbles around the host star(s). This is backed up by more recent work such as Fierlinger et al. (2016). Observational evidence for wind-driven bubbles is given by hot X-ray emission (e.g Dunne et al. 2003), which requires hot gas above 10^6 K shocked by highly energetic kinetic flows. However, if most of this energy is lost to radiative cooling (see Mac Low & McCray 1988), the influence of winds is strongly diminished.

The transition from purely adiabatic to efficiently cooling winds is discussed in the context of H II regions by Rahner et al. (2017), Silich & Tenorio-Tagle (2018), and Rahner et al. (2019), where the cooling rate of winds greatly affects their ability to drive an expanding shell. Silich & Tenorio-Tagle (2017) additionally argue that if the wind bubbles around individual stars do not merge, the combined effect of winds is further reduced. Harper-Clark & Murray (2009) and Krumholz & Matzner (2009) also argue that winds can easily escape a porous shell owing to their high velocities. This causes a further reduction in the ability for winds to drive a spherical shell outwards.

1.3 Radiation pressure

Radiation pressure from photons of various energies has been proposed as a mechanism for driving flows in astrophysical environments. Mathews (1967), Krumholz & Matzner (2009), Murray, Quataert & Thompson (2010), Draine (2011), and Kim, Kim & Ostriker (2016) have highlighted the role of radiation pressure in driving the expansion of H II regions. The structure of H II regions with strong sources of radiation pressure is complex. Pellegrini et al. (2007) and Pellegrini et al. (2009) argue that radiation pressure sets up a density gradient in H II regions due to the differential flux of ionizing photons throughout the H II region.

In this paper we do not include low-energy photons. This is because Reissl et al. (2018) showed that infrared photons are unable to couple to the ISM, and thus cannot strongly influence the evolution of H II regions. The reason is that photons shift to lower energies as they are absorbed and remitted at longer wavelengths by dust, decreasing their momentum transfer rate over time in all but the most massive clouds. Rahner et al. (2017) further considered a full range of feedback forces and found that when properly accounting for opacity in dynamic models, IR radiation pressure was at most a small perturbation.

1.4 Interacting processes

Various works have been done to describe the interaction between winds and photoionized H II regions. Dyson (1977) used adiabatic wind solutions to trace the expansion of blister H II regions with embedded winds, while Capriotti & Kozminski (2001) produced more detailed solutions for winds and a photoionized H II region in a uniform external medium, finding that winds are very rarely

the principal drivers of the expansion. Krumholz & Matzner (2009) performed an analysis of various modes of feedback by comparing them to the Spitzer (1978) solution for a D-type photoionized H II region in a uniform medium, while Haworth et al. (2015) did the same for the detailed microphysics driving D-type H II regions.

Haid et al. (2018) found good agreement between simple analytic models and simulations of H II regions and stellar winds in uniform environments. In their paper, as well as the model of Krumholz & Matzner (2009) and the simulations of Dale et al. (2014), photoionization is the most important process to capture in most dense cloud environments studied. Outside the cloud, however, they argue that photoionization should have a minimal effect since background radiation will heat the diffuse gas to temperatures near the equilibrium temperature of photoionized gas.

A simple approach previously employed has been to add the pressures from each dynamical process driving feedback bubbles as if they acted independently from the other forces, for example by Murray et al. (2010). This is a reasonable assumption if all but one process is negligible at a given time, but breaks down if complex interactions are considered. For example, as in Pellegrini et al. (2007), while radiation pressure adds a force that is propagated to the edge of the H II region, the departure from a constant density H II region increases the recombination rate of the H II region, shrinking the radius of the region as a result. Since a full physical model has no linear algebraic solution, various numerical analytic solutions exist that capture the various physics involved (e.g. Pellegrini et al. 2009; Yeh & Matzner 2012; Verdolini et al. 2013; Rahner et al. 2017).

We conclude that H II regions are complicated phenomena that require careful consideration in order to avoid oversimplifying assumptions about their structure and dynamics. In this paper we focus specifically on how winds and radiation pressure shape photoionized H II regions expanding into self-gravitating power-law gas density fields, treating each process as perturbations to our dynamical equations. We calculate where such perturbations should become large enough to demand more complicated numerical solutions.

1.5 Paper outline

We start by briefly outlining the conceptual structure of an H II region in Section 2. We then give equations used to describe the cloud into which the H II region expands in Section 3. In Section 4, we introduce a set of formulae to describe the expansion of ionization fronts driven purely by photoionization. We then derive corrections to these expressions to account for the role of winds (Section 5), radiation pressure (Section 6), photon breakout and gravity (Section 7). For each additional effect we calculate a coefficient that characterizes how important the effect is compared to a solution without that effect. We then compute solutions to the problem using physically motivated cloud properties and stellar evolution models. In Section 8 we describe how we set up these models, and in Section 9 we summarize the results of these solutions. Finally, we discuss the context and significance of our findings in Section 10.

2 A TYPICAL H II REGION

In this section we summarize the components of an H II region to illustrate how our model is constructed. We do not provide details or justifications for model choices in this section, but link to the parts of the text where each effect is discussed in more detail.

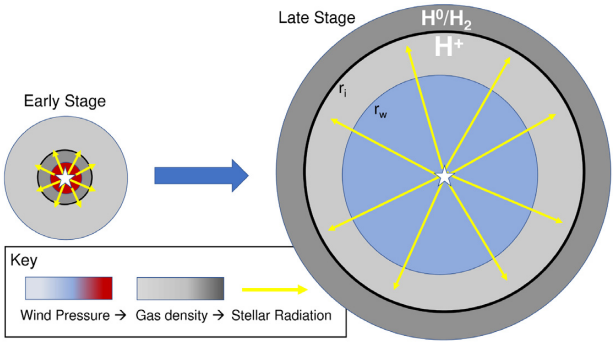

Figure 1. Schematic showing the components of the modelled H II region. Figure adapted with permission from Rahner et al. (2017).

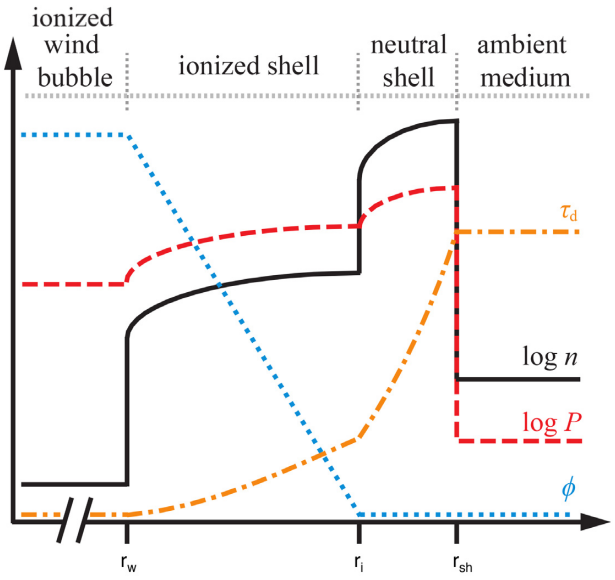

Figure 2. Schematic showing the typical density (n), pressure (P), ionizing photon flux (ϕ), and optical depth of the dust ($\tau_{\rm d}$) profiles in the H II region and outside. Figure adapted with permission from Rahner et al. (2017).

The structure of an H II region is illustrated in Fig. 1. Typical radial distributions of density n, pressure P, photon flux ϕ, and optical depth $\tau_{\rm d}$ are given in Fig. 2. The radial components of this profile are as follows:

(i) At $r = 0, t = 0$, the OB star or cluster of stars forms at a density peak in a volume of dense, neutral cloud material (Section 3).

(ii) Stellar winds have the same temperature as the surface of the star, reaching terminal velocities of 1000–3000 km s^{-1} (see Section 8.3). This material shocks against the ambient medium, creating a bubble of hot, diffuse, collisionally ionized gas out to radius $r_{\rm w}$ (Section 5).

(iii) Ionizing UV photons are emitted from the star. They pass through the collisionally ionized wind bubble and photoionize a volume of gas from $r_{\rm w}$ to $r_{\rm i}$. A typical assumption is that these regions have a constant density (Section 4). Radiation pressure introduces a density gradient in the H II region, which in certain regimes cannot be ignored (see Section 6.2 for a discussion).

(iv) A dense, neutral shell is swept up between $r_{\rm i}$ and $r_{\rm sh}$, beyond which lies the unshocked cloud material. If sufficient photons are emitted, this shell can become fully ionized, causing photons to break out of the H II region and stream into the external medium

(Section 7.1). $r_{\rm sh}$ can also shrink via self-gravity or accretion from the external medium (Section 7.2). In this paper we assume that $r_{\rm sh} \simeq r_{\rm i}$.

3 HOST ENVIRONMENT OF THE H II REGION

In this section we discuss the density distribution of the initially neutral gas into which the H II region expands.

3.1 A power-law density profile

The majority of massive stars are thought to form in molecular clouds. These objects have been widely studied in the literature to date (see reviews by Mac Low & Klessen 2004; Ballesteros-Paredes et al. 2007; Hennebelle & Falgarone 2012; Klessen & Glover 2016). They are often modelled as fractal structures based on analysis of observed clouds (Cartwright & Whitworth 2004; Hennebelle & Falgarone 2012; Li et al. 2015; Jaffa et al. 2018). Larson (1981) argues for a hierarchy of overdensities with defined power-law relations in size, mass, density, and velocity dispersion. These overdensities collapse under gravity, and form peaked density profiles inside which protostars form.

In the recent simulations of Lee & Hennebelle (2018), star-forming cores are found to have a roughly power-law density profile $n \propto r^{-w}$ where $w \simeq 2$, otherwise called a singular isothermal sphere. Observational studies by Kauffmann et al. (2010) find a similar trend, based on inference from 2D column density maps. This profile has also been used in previous theoretical studies of H II regions, e.g. by Shu et al. (2002) and Alvarez et al. (2006) among others.

In this section and Section 4 we give solutions for an arbitrary w. In order to provide tractable solutions, sections after that all assume $w = 2$. We ignore the role of accretion in changing the form of this profile, and assume that once the H II region forms its expansion is rapid enough to neglect additional mass from outside accretion. Future use of these models should explore this issue.

We define the density profile of the cloud

$$n(r) = n_0 (r/r_0)^{-w}, \tag{1}$$

where $n(r)$ is the number density of the cloud at radius r and time t, w is the exponent of the power law, n_0 and r_0 are a characteristic number density and radius. The quantities r_0^w and n_0 are degenerate. In this paper we use r_0 as some arbitrary boundary at which we measure the cloud properties, and so $n_0 = n(r_0)$.

The mass density of the cloud is given by

$$\rho(r) = n(r) \frac{m_{\rm H}}{X}, \tag{2}$$

where $m_{\rm H}$ is the mass of a hydrogen atom and X is the hydrogen mass fraction. The mass of the cloud (ignoring any central stellar mass) integrated out to a radius r is then

$$M(<r) = \frac{4\pi}{3-w} n_0 r_0^w r^{3-w} \frac{m_{\rm H}}{X}. \tag{3}$$

Lombardi, Alves & Lada (2010) argue that structures inside observed nearby molecular clouds are defined by mass contained within a given cut-off surface density $\Sigma(r)$. At radius r and for $w = 2$, $\Sigma(r)$ is given by

$$\Sigma(r) = \pi n_0 r_0^2 r^{-1} \frac{m_{\rm H}}{X} \tag{4}$$

(see Binney & Tremaine 2008). Defining $\Sigma_0 \equiv \Sigma(r_0)$ and $M_0 \equiv M(<r_0)$, we can write for $w = 2$:

$$n_0 r_0^2 \frac{m_{\rm H}}{X} = \frac{1}{2\pi} (M_0 \Sigma_0)^{1/2}. \tag{5}$$

The mass inside radius r then becomes

$$M(<r) = 2 (M_0 \Sigma_0)^{1/2} r. \tag{6}$$

We can solve these equations to relate r_0 and n_0 to Σ_0 and M_0:

$$r_0 = \frac{1}{2} \sqrt{\frac{M_0}{\Sigma_0}}, \tag{7}$$

$$n_0 = \frac{2}{\pi} \frac{X}{m_{\rm H}} M_0^{-1/2} \Sigma_0^{3/2}. \tag{8}$$

4 THERMAL EXPANSION OF A CONSTANT DENSITY PHOTOIONIZED H II REGION

In this section we introduce our model for the behaviour of photoionization fronts in self-gravitating power-law density profiles without winds or radiation pressure. See Section 1.1 for a discussion of previous analytic work on this topic.

In addition to the power-law structure of the neutral cloud in equation (1), we must invoke two additional conditions: (1) that the H II region contained within the photoionization front is in photoionization equilibrium, (2) and the thermal pressure of the photoionized gas is balanced by the ram pressure on the shell from the external medium. In Section 7.1 we discuss when these conditions break down.

Condition (1), photoionization equilibrium, is satisfied by

$$\frac{4\pi}{3} r_i^3 n_i^2 \alpha_{\rm B} = Q_{\rm H} \tag{9}$$

as discussed by Strömgren (1939), where $r_{\rm i}$ is the radius of the photoionization front, $n_{\rm i}$ is the number density in the photoionized gas, $\alpha_{\rm B}$ is the recombination rate of the photoionized gas (=2–3 $\times$ 10^{-13} cm^3 s^{-1} in typical solar conditions), and $Q_{\rm H}$ is the emission rate of ionizing photons. In this section, as in Spitzer (1978) and others, we assume that the density in the photoionized gas is constant due to thermal mixing. In these calculations we typically assume that the ions are well represented by singly ionized hydrogen. We ignore a small correction in the electron number density due to multiple ionization of helium, metal species, and dust. In this section we ignore the effects of radiation pressure, which we discuss in Section 6.

Condition (2), pressure equilibrium, is given by

$$n_{\rm i} c_{\rm i}^2 = n(r_{\rm i}) (\dot{r}_{\rm i} + v_0)^2, \tag{10}$$

where $c_{\rm i}$ is the isothermal sound speed in the photoionized gas (of the order of 10 km s^{-1} for gas at 10^4 K), $n(r_{\rm i})$ is a power law defined as in equation (1), and v_0 is a generic term used to describe pressure forces from gravity and accretion flows from the external medium on to the shell as in Raga et al. (2012). We assume that all velocities are in the radial direction and so values of v_0 are negative, representing either a resistive force on the expansion or accretion on to the shell. In Appendix A we derive forms for this v_0, which is independent of r.

We define a stall radius $r_{\rm stall}$ where $\dot{r}_i = 0$, and introduce a scale-free radius $R \equiv r_{\rm i}/r_{\rm stall}$ (and $\dot{R} \equiv \dot{r}_{\rm i}/r_{\rm stall}$). Solving these equations (see Appendix B) gives

$$\dot{r}_{\rm i} = v_0 (R^{\frac{2w-3}{4}} - 1). \tag{11}$$

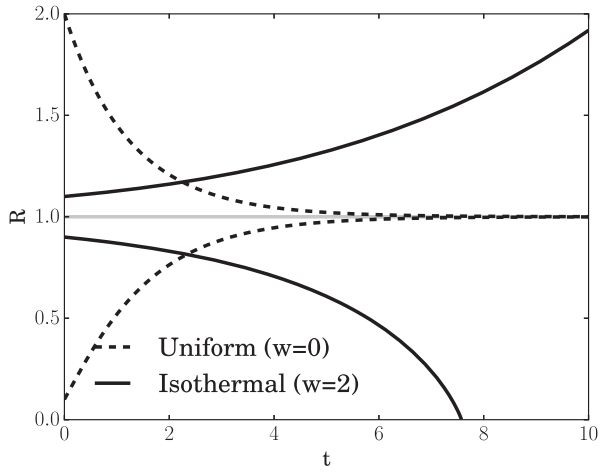

Figure 3. Solutions to equation (11) for the expansion of an H II region with a ram pressure term based on gravity or accretion using scale-free units. Here, $r_{\rm stall} = r_{\rm launch} = 1$ (grey solid line) and $v_0 = R^{1-w/2}$. This figure demonstrates that in the case of a uniform gas field, $r_{\rm stall}$ is a *stable* point which solutions converge to. For steeper potentials, the solution tends to zero or infinity, i.e. $r_{\rm stall}$ is an *unstable* point. $r_{\rm stall}$ is thus no longer a true 'stall' point, but instead a launching radius $r_{\rm launch}$.

In a uniform medium ($w = 0$), this equation has a *stable* point at $r_{\rm stall}$, where R will tend to 1 over time. Note that v_0 is of the order of the escape velocity $\sqrt{2GM/R}$. Using equation (3), this gives $v_0 \propto R^{1-w/2}$. v_0 is thus constant with R where $w = 2$.

For $w > 3/2$, the exponent $(2w - 3)/4$ in equation (11) becomes positive. Under these conditions, $r_{\rm stall}$ becomes an *unstable* equilibrium point in a *bistable* system with attractors at $R = 0$ and infinity. *In other words, the ionization front will either accelerate forever or be crushed depending on the initial radius of the photoionization front*. We illustrate this behaviour in Fig. 3.

Under these conditions, $r_{\rm stall}$ is no longer a true 'stall' point, but instead a 'launching' radius, $r_{\rm launch} \equiv r_{\rm stall}$. In other words, if $r > r_{\rm launch}$, the solution will accelerate over time. We use this terminology for the rest of the paper, since we focus largely on profiles where $w = 2$.

In Appendix B, we derive equation (11) in terms of $t_{\rm ff,0}$, which is the freefall time at density n_0 where $w = 2$:

$$\dot{R} = R_0 \frac{\pi}{2} \frac{\sqrt{3f}}{t_{\rm ff,0}} (R^{1/4} - 1), \tag{12}$$

where $R_0 \equiv r_0/r_{\rm launch}$ and $f \equiv (v_0/v_{\rm esc})^2$.

The free-fall time $t_{\rm ff,0}$ is thus a significant factor in setting the time-scale for the expansion of the H II region (see also Geen et al. 2016).

5 WINDS IN UV PHOTOIONIZED BUBBLES

Stellar winds are outflows of material from stars driven by radiation from inside the star. Winds from massive stars reach a terminal velocity of 1–4 times the escape velocity at the surface of the star (e.g. Vink et al. 2011). This velocity can be well over 1000 km s^{-1}.

The winds initially free-stream but at some radius shock against the ambient medium. The temperature of the shocked gas is typically above 10^6 K, and the temperature of the thermalized gas is in pressure equilibrium with the speed of the free-streaming phase (see e.g. Weaver et al. 1977, for a discussion of this transition).

Since the temperature of this gas is typically well above the limit to be collisionally ionized, the UV photons from the star are not absorbed by the wind bubble. The wind is thus always embedded inside a photoionized volume, although for strong winds and weak ionizing sources, the photoionized region can be a thin shell around a wind-blown bubble.

In this section we first discuss how winds affect the structure of photoionized H II regions. We then calculate the relative impact of winds and photoionization on the dynamics of H II regions. To provide tractable solutions, all further equations in this paper take $w = 2$.

5.1 Pressure from stellar winds

We have a stellar source with mass-loss rate $\dot{m}_{\rm w}$ and terminal velocity $v_{\rm w}$. This gives us a wind luminosity $L_{\rm w} \equiv \frac{1}{2}\dot{m}_{\rm w} v_{\rm w}^2$ and a wind momentum deposition rate $\dot{p}_{\rm w} \equiv \dot{m}_{\rm w} v_{\rm w}$.[1]

There are two models for the pressure exerted by stellar winds on to an external medium given by Silich & Tenorio-Tagle (2013). In the first, energy-conserving model, minimal radiative losses are assumed as in Weaver et al. (1977), and the bubble is supported by thermalized gas that stores the energy emitted by the stellar source over its lifetime,

$$P_{\rm w,e} = \left(\frac{k_{\rm w}^2 L_{\rm w}^2 \rho_{\rm i}}{r_{\rm w}^4} \right)^{1/3}, \tag{13}$$

where $r_{\rm w}$ is the radius of the wind bubble, $\rho_{\rm i}$ is the mass density in the ionized gas $n_{\rm i} m_{\rm H}/X$, and $k_{\rm w}$ is a constant dependent on the adiabatic index γ in the wind bubble,

$$k_{\rm w}^2 = \frac{7}{25} \left(\frac{375(\gamma - 1)}{28\pi(9\gamma - 4)} \right)^2. \tag{14}$$

In the second, momentum-conserving model, the wind bubble cools strongly due to the high density of the gas. Storage of energy from previous wind emission is minimal. The outward force instead comes directly from the momentum injection rate of the star. This model is given by

$$P_{\rm w,m} = \frac{\dot{p}_{\rm w}}{4\pi r_{\rm w}^2}. \tag{15}$$

The precise pressure from the wind bubble will lie somewhere between these two solutions (see e.g. Silich & Tenorio-Tagle 2018). If the cooling time is much longer than the lifetime of the stellar source, the energy-conserving solution will apply. Mac Low & McCray (1988) argue that this condition applies for galactic superbubbles in more diffuse media. For much denser environments, where the cooling time is much shorter than the lifetime of the stellar source, the momentum-conserving solution is more applicable. The cooling time-scale for the wind bubble is given in Mac Low & McCray (1988) as

$$t_{\rm c} = (2.3 \times 10^4 {\rm yr}) n_{\rm i}^{-0.71} (L_{\rm w}/10^{38} {\rm erg\,s^{-1}})^{0.29} \tag{16}$$

assuming that the wind bubble is expanding into the photoionized region with a density of $n_{\rm i}$ and the main cooling mode is mixing with the background material.

To get an estimate of how much $n_{\rm i}$ is reduced with respect to the external density field with a $1/r^2$ profile, we can use equations (1)

[1]Throughout this paper, small p denotes a momentum term, and large P a pressure term.

and (9) to write

$$\frac{n_\mathrm{i}}{n(r_\mathrm{i})} = \left(\frac{3Q_\mathrm{H}r_\mathrm{i}}{4\pi\alpha_\mathrm{B}}\right)^{1/2}\frac{1}{n_0 r_0^2}. \quad (17)$$

If we take $r_\mathrm{i} = r_0$, this ratio is above 0.1 for typical values used in this work. The internal density of the H II region is thus not significantly reduced compared to the external density. This is because the H II region expands into a cloud with a density profile that decreases with radius, and so the photoionized gas remains at a high density compared to its surroundings. In a uniform region, where the external density does not change, the Spitzer (1978) solution leads to much lower values of $n_\mathrm{i}/n(r_\mathrm{i})$ over time. See Section 9.1 for an example of the evolution of n_i around a single massive star.

The values of t_c at molecular cloud densities is typically short, of the order of 1–10 kyr. We expect the momentum-driven pressure in equation (15) to be more representative under the conditions considered in this paper, and use this form from now on. An algebraic model with fully self-consistent radiative cooling is difficult to obtain. Rahner et al. (2019) recently calculated a semi-analytic solution that treats the out-of-photoionization-equilibrium radiative cooling in H II regions with wind bubbles, which accurately models the transition from adiabatic to radiatively cooled winds. This is likely to be most important in the early stage of the H II region evolution or in more diffuse regions where the density is lower, as in Mac Low & McCray (1988). Rahner et al. (2019) also treat the long-term evolution of H II regions after the first supernovae have occurred, which we omit in this work.

5.2 Evolution inside H II regions

Since the sound speed in the wind bubble is much higher than the sound speed in the photoionized gas (>1000 km s^{-1} versus ∼10 km s^{-1}), we assume that r_w reaches its equilibrium state quickly compared to the expansion rate of the photoionization bubble. The radius of the wind bubble r_w is thus always balanced by hydrostatic equilibrium between the wind pressure and the thermal pressure of the photoionized gas.

We modify equation (9) to account for the collisionally ionized wind bubble inside the H II region

$$\frac{4\pi}{3}n_\mathrm{i}^2\left(r_\mathrm{i}^3 - r_\mathrm{w}^3\right)\alpha_\mathrm{B} = Q_\mathrm{H}. \quad (18)$$

The pressure condition on the external medium in equation (10) remains valid when a wind bubble is included, since the wind bubble is contained entirely within the photoionized H II region. The pressure from the wind in equation (15) (or equation 13 in the energy-conserving case) balances the pressure in the photoionized gas as

$$P_\mathrm{w} = n_\mathrm{i}c_\mathrm{i}^2\frac{m_\mathrm{H}}{X}. \quad (19)$$

In the momentum-conserving phase, this gives

$$\frac{\dot{p}_\mathrm{w}}{4\pi r_\mathrm{w}^2} = n_\mathrm{i}c_\mathrm{i}^2\frac{m_\mathrm{H}}{X}. \quad (20)$$

We can substitute these equations (see Appendix C) as

$$(\dot{r}_\mathrm{i} + v_0)^4 = A_\mathrm{w}(\dot{r}_\mathrm{i} + v_0) + A_\mathrm{i}r_\mathrm{i}, \quad (21)$$

where A_w and A_i are constants relating to the wind and photoionization, respectively:

$$A_\mathrm{w} = \left(\frac{\dot{p}_\mathrm{w}}{4\pi}\frac{X}{m_\mathrm{H}}\right)^{3/2}\left(n_0 r_0^2\right)^{-3/2} \quad (22)$$

and

$$A_\mathrm{i} = \frac{Q_\mathrm{H}}{\alpha_\mathrm{B}}\frac{3}{4\pi}\left(c_\mathrm{i}^2\right)^2\left(n_0 r_0^2\right)^{-2}. \quad (23)$$

In Appendix A we show that for a $1/r^2$ density profile, v_0 is constant. This means that the expansion rate r_i of the H II region is reduced by a constant factor v_0 at all times.

5.3 How important are winds dynamically?

When the contribution from winds is equal to the contribution from photoionization, we can write equation (21) as

$$(\dot{r}_\mathrm{ieq} + v_0)^4 = 2A_\mathrm{i}r_\mathrm{i} = 2A_\mathrm{w}(\dot{r}_\mathrm{ieq} + v_0), \quad (24)$$

where $\dot{r}_\mathrm{ieq}$is the expansion rate under these conditions.

We can define a factor C_w as the ratio of the contribution from winds and photoionization. $C_\mathrm{w} < 1$ if photoionization is the principal driver in equation (21), and $C_\mathrm{w} > 1$ if winds are the principal driver. If equation (24) applies, $C_\mathrm{w} = 1$. Around this limit

$$C_\mathrm{w} \equiv \frac{A_\mathrm{w}(\dot{r}_\mathrm{i} + v_0)}{A_\mathrm{i}r_\mathrm{i}} \simeq \frac{A_\mathrm{w}(2A_\mathrm{i}r_\mathrm{i})^{1/4}}{A_\mathrm{i}r_\mathrm{i}}$$
$$= 2^{1/4}A_\mathrm{w}(A_\mathrm{i}r_\mathrm{i})^{-3/4}. \quad (25)$$

This can be expanded using equations (22) and (23) to the form

$$C_\mathrm{w} = 2^{1/4}\left(\frac{\dot{p}_\mathrm{w}}{4\pi}\frac{X}{m_\mathrm{H}}\frac{1}{c_\mathrm{i}^2}\right)^{3/2}\left(\frac{Q_\mathrm{H}}{\alpha_\mathrm{B}}\frac{3}{4\pi}r_\mathrm{i}\right)^{-3/4}. \quad (26)$$

Setting $r_\mathrm{i} = r_0$, we can calculate the relative effect of winds versus photoionization in driving the expansion of an H II region by the time it reaches a characteristic radius r_0 enclosing a mass M_0 with bounding surface density Σ_0, using fiducial values for the terms in equation (26) as listed in Section 8:

$$C_\mathrm{w} = 0.009\,31\left(\frac{\dot{p}_\mathrm{w}}{10^{28}\ \mathrm{g\,cm\,s^{-2}}}\right)^{3/2}\left(\frac{Q_\mathrm{H}}{10^{49}\ \mathrm{s^{-1}}}\right)^{-3/4}$$
$$\times\left(\frac{M_0}{100\ \mathrm{M_\odot}}\right)^{-3/8}\left(\frac{\Sigma_0}{100\ \mathrm{M_\odot\,pc}}\right)^{3/8}\left(\frac{c_\mathrm{i}}{10\ \mathrm{km\,s^{-1}}}\right)^{-3}. \quad (27)$$

The relative impact of winds depends on the factor $\dot{p}_\mathrm{w}^2/Q_\mathrm{H}$. In other words, for a given stellar evolution model, the relative impact of winds grows as stars are added (i.e. where both quantities increase linearly).

5.4 Ratio of radii of wind and photoionization bubbles

Substituting equations (20) and (26) into equation (18), we can find a relationship for the ratio between the radius of the photoionization bubble r_i and the radius of the wind bubble r_w. Note that r_i is the radius of the H II region as a whole, since the ionizing photons always pass through the collisionally ionized wind bubble:

$$\left(\frac{r_\mathrm{i}}{r_\mathrm{w}}\right)^4 = 2^{1/3}C_\mathrm{w}^{-4/3} + \frac{r_\mathrm{i}}{r_\mathrm{w}}. \quad (28)$$

For large values of C_w, $r_\mathrm{w} \to r_\mathrm{i}$. At $C_\mathrm{w} = 1$, $r_\mathrm{w}/r_\mathrm{i} = 0.79$. At $C_\mathrm{w} = 0.1$, this drops to $r_\mathrm{w}/r_\mathrm{i} = 0.43$, while $C_\mathrm{w} = 10$ gives $r_\mathrm{w}/r_\mathrm{i} = 0.98$. A reasonably large wind bubble can therefore exist even if winds are not dynamically significant, while for cases where winds are the main driver of the H II region, the wind bubble will occupy most of the volume of the H II region. A large wind bubble is therefore not always an indicator that winds are dynamically important.

5.5 Density of photoionized gas

By substituting the expression for r_w derived from equation (20) into equation (18), we can write the density of the photoionized gas as

$$n_i^2 r_i^3 = \left(\frac{\dot{p}_w}{4\pi}\frac{X}{m_H}\frac{1}{c_i^2}\right)^{3/2} n_i^{1/2} + \frac{Q_H}{\alpha_B}\frac{3}{4\pi}. \quad (29)$$

In the absence of stellar wind, this becomes equation (9) describing photoionization equilibrium where the photoionized gas fills the spherical volume enclosed by r_i ($n_i \propto r_i^{-3/2}$). If, however, winds become the principal driver of the H II region (i.e. the second term in the right-hand side of equation 29 is neglected), we obtain $n_i \propto (4\pi r_i^2)^{-1}$. In these conditions, $r_w \to r_i$ and the photoionized gas is confined to a thin shell at r_i.

We discuss the observational significance of the changes to the radial structure and density of the H II region in Section 10.4.

6 RADIATION PRESSURE

The role of radiation pressure from ionizing photons is different from stellar winds. Rather than acting on the inner surface of the photoionized region, radiation pressure distributes itself throughout the photoionized gas. In this section we calculate the relative effect of adding a radiation pressure term to the solutions derived in the paper so far. We treat radiation pressure as a perturbation to the constant-density H II region model and discuss what happens when this perturbation grows to non-negligible levels.

6.1 Relative importance of radiation pressure

We introduce a quantity C_{rp} to track the effect of radiation pressure as a perturbation to the photoionization-driven solution. We use a similar method to Krumholz & Matzner (2009), who consider the addition that radiation pressure makes to the total pressure from the H II region at r_i. Krumholz & Matzner (2009) write the total additional pressure from radiation acting on the H II region at r_i as

$$\Delta P_{rp} = \frac{f_{trap} L}{4\pi r_i^2 c}, \quad (30)$$

where L is the total bolometric luminosity of the star and f_{trap} is a boosting factor to account for multiple scattering of photons. For significant losses of photons, f_{trap} can be less than 1. We calculate whether the escape of ionizing photons occurs in Section 7.1.

L can be written in terms of the ionizing photon output as

$$L = \psi \langle h\nu \rangle Q_H, \quad (31)$$

where $\langle h\nu \rangle$ is the average energy of photons emitted by the star and ψ is a factor that accounts for the fraction of the spectrum below 13.6 eV. Krumholz & Matzner (2009) adopt $\psi = 1$ in the case of output from massive stars, which emit significant quantities of ionizing radiation.

Setting P_0 to the thermal pressure in the H II region from photoionization using equation (19), we can write

$$C_{rp} \equiv \frac{\Delta P_{rp}}{P_0} = \frac{Q_H}{4\pi r_i^2}\frac{f_{trap}\langle h\nu \rangle}{c}\left(c_i^2 \frac{m_H}{X}\right)^{-1}\frac{1}{n_i}. \quad (32)$$

In the absence of winds, this becomes

$$C_{rp,nowind} = \left(\frac{Q_H}{12\pi\alpha_B\phi_d}\right)^{1/2}\frac{f_{trap}\langle h\nu \rangle}{c}\left(c_i^2\frac{m_H}{X}.\right)^{-1} r_i^{-1/2}. \quad (33)$$

A term ϕ_d is introduced to account for losses to photoionized gas pressure from dust. This is equivalent to equation 7 in Krumholz & Matzner (2009), who compute C_{rp} in terms of n_i rather than r_i. We adopt a fiducial $f_{trap} = 2$ and $\phi_d = 0.73$ from Krumholz & Matzner (2009) (a more accurate estimate of these quantities requires a numerical solution to the full radiative transfer equations). Equation (33) can thus be written as

$$C_{rp,nowind} = 0.047\left(\frac{\langle h\nu \rangle}{13.6\,\mathrm{eV}}\right)\left(\frac{c_i}{10\,\mathrm{km\,s^{-1}}}\right)^{-2}\left(\frac{Q_H}{10^{49}\,\mathrm{s^{-1}}}\right)^{1/2} \times \left(\frac{r_i}{1\,\mathrm{pc}}\right)^{-1/2}. \quad (34)$$

As in Krumholz & Matzner (2009), radiation pressure is most important in small H II regions with high-luminosity sources.

In Section 9, we solve for C_{rp} using equation (32) at a given r_i and n_i. We use equation (20) to calculate n_i, which requires equation (28) to calculate r_w. Equation (28) does not have a simple algebraic solution, so we rely on a numerical solution to this particular equation. We discuss the effects of the inclusion of a wind bubble on the calculation of C_{rp} in Section 9.1.

6.2 H II regions with strong radiation pressure

As the relative strength of radiation pressure increases, the structure of the H II region changes. For increasing radius r inside r_i, radiation pressure accumulates. This must in turn be balanced by increasing density as $r \to r_i$. For cases with very strong radiation pressure, as in small or very dense regions, most of the material in the H II region is pushed towards a thin shell at r_i. This in turn allows the wind bubble to expand outwards. The combination of these equations is complex and requires a numerical solution (Pellegrini et al. 2007, 2009).

A parameter space exploration using numerical solutions for H II regions with radiation pressure is given in Draine (2011). They do not include stellar winds but do include dust and non-ionizing radiation. In fig. 5 of their paper, they give parameters for where the RMS density of the H II region diverges significantly from the mean density (i.e. the H II region can no longer be considered uniform density). Such density gradients are also visible in papers that compute numerical solutions including winds, magnetic fields, self-gravity, and other effects (e.g. Pellegrini et al. 2007; Yeh & Matzner 2012; Rahner et al. 2019).

For values where C_{rp} approaches 1, we expect winds and radiation pressure to move the H II region's structure and evolution away from a simple algebraic solution. In this regime, a numerical solution is required. In Section 9 we give the parameter space where this is likely to happen.

The precise values of f_{trap}, ϕ_d, and ψ affect how effective radiation pressure is. This is not a trivial thing to calculate. In this work we pick fiducial values from Krumholz & Matzner (2009), but there is still debate in the literature about how efficiently radiation pressure from photons is coupled to the gas. The simulations of Krumholz & Thompson (2012) and Krumholz & Thompson (2013), for example, show that instabilities generated in the gas and dust create cavities that allow radiation to escape more efficiently, reducing f_{trap}. Davis et al. (2014) and Rosdahl & Teyssier (2015) confirm this with similar calculations using different radiation tracing methods. These effects are particularly important when considering the contribution of infrared photons. By contrast, the simulations of Kimm et al. (2019) show that Lyman alpha (Ly α) photons can be generated through recombination of other ionizing photons and scatter very efficiently, which in principle would boost f_{trap}. Photoelectric heating of dust grains has also been proposed as a feedback mechanism (Forbes

et al. 2016). Radiation is thus a complex subject that requires careful modelling.

In the next section we discuss the role of gravity and photon breakout on the H II region.

7 PHOTON BREAKOUT AND GRAVITY

In this section we review additional terms presented in other work that affect the ionization front. First, we discuss the inability for the D-type solution to contain the ionizing photons leading to rapid photoionization of the whole clump/cloud. Secondly, we discuss the cases where gravity and accretion are able to stop the expansion of the H II region.

7.1 Photon breakout

Franco et al. (1990) argue that for power-law external density fields where $w > 3/2$, runaway photoionization occurs, leading to a 'champagne' flow that rapidly photoionizes the entire cloud. If some processes such as stellar winds create an initial dense shell, a D-type H II region can be contained even in steeper density fields than this. However, once the champagne flow phase begins, the ionization front expands in the R-type mode (Kahn 1954), which is solved in the relativistic limit by Shapiro et al. (2006). After this point, the whole cloud is overtaken by the ionization front and expands thermally at a few times the speed of sound in the photoionized gas (see equation 24 in Franco et al. 1990).

Alvarez et al. (2006) find the limit where this occurs, assuming the internal structure of the H II region derived by Shu et al. (2002) in a $w = 2$ cloud (we assume a similar density field for most of this paper). We can rewrite equation 5 in Alvarez et al. (2006) for the radius at which the ionization front breaks out of the D-type phase and enters a champagne phase $r_{\rm B}$, in terms of M_0 and Σ_0 as

$$r_{\rm B} = 0.75\ {\rm pc} \left(\frac{M_0}{100\ {\rm M}_\odot}\right) \left(\frac{\Sigma_0}{100\ {\rm M}_\odot\ {\rm pc}^{-2}}\right) \times \left(\frac{Q_{\rm H}}{10^{49}\ {\rm s}^{-1}}\right)^{-1} \left(\frac{c_{\rm i}}{10\ {\rm km\,s}^{-1}}\right)^{4}. \quad (35)$$

Comparing this to the radius of the cloud r_0 (see equation 7) and derive a ratio $C_{\rm B} \equiv r_0/r_{\rm B}$,

$$C_{\rm B} = 0.8 \left(\frac{M_0}{100\ {\rm M}_\odot}\right)^{-1/2} \left(\frac{\Sigma_0}{100\ {\rm M}_\odot\ {\rm pc}^{-2}}\right)^{-3/2} \times \left(\frac{Q_{\rm H}}{10^{49}\ {\rm s}^{-1}}\right) \left(\frac{c_{\rm i}}{10\ {\rm km\,s}^{-1}}\right)^{-4}, \quad (36)$$

where $C_{\rm B} > 1$ means that a breakout occurs before the ionization front reaches r_0, assuming a Shu et al. (2002) solution for the photoionized gas. This is possible in small clouds with low surface densities and strong ionizing photon sources with a low ionizing sound speed. We give some physical scenarios for this in Section 9. The steep power-law dependence on $c_{\rm i}$ means that efficient cooling found at supersolar metallicities may also allow a breakout.

We do not provide an algebraic form for the photon escape fraction from the H II region in the presence of winds, radiation pressure and radiative cooling, since this requires complex numerical solutions such as those given by Rahner et al. (2017). Instead, we offer the following comments:

(i) Photon leakage depends on the integration of $n(r, t)^2$ out to the ionization front, including the shell around the ionization front. This is governed by radiative cooling out of photoionization equilibrium (as well as any non-spherical geometry, ignored here). Since winds drive the early expansion of the H II region (c.f. equation 21), a dense shell can already have formed, which will more effectively trap the H II region.

(ii) Photon leakage does not immediately cause photoionization to become ineffective, since the wind must still expand into a dense, albeit photoionized cloud. In both cases the ionization front expands rapidly (faster than $c_{\rm i}$).

(iii) Once the entire cloud has been ionized and $r_{\rm i}$ enters the warm interstellar medium (WIM), there will be no well-defined H II region boundary. Instead, only a wind-blown bubble may be observable as a distinct object, creating the misleading impression that the feedback from the star is driven solely by winds.

(iv) We neglect here the role of fragmentation, which is included in the semi-analytic model of Rahner et al. (2019).

7.2 The role of gravity and accretion

In this section we discuss the role of resistive forces such as gravity and ram pressure from accretion on the shell around the ionization front, which we have to this point characterized as a velocity term in the dynamical equations. In Appendix A we derive forms for these terms.

In Section 4, we establish that in a $w = 2$ density profile, the stall radius becomes a 'launching radius' $r_{\rm launch}$, above which $r_{\rm i}$ accelerates over time. Rearranging equation (21) and setting $\dot{r}_{\rm i} = 0$ and $r_{\rm i} = r_{\rm launch}$ (for the sake of simplicity we neglect radiation pressure), we arrive at

$$r_{\rm launch} = \frac{v_0 \left(v_0^3 - A_{\rm w}\right)}{A_{\rm i}}. \quad (37)$$

There is no good scale-free way to characterize $r_{\rm launch}$ and determine whether the ionization front will expand or be crushed, since this criterion depends on smaller scales governing evolution of the H II region than we study here. We plot characteristic values for $r_{\rm launch}$ in Section 9 and discuss further what this means for the evolution of the H II regions.

In Appendix D we calculate the ability for self-gravity inside the H II region to set up a density gradient, similar to radiation pressure in Section 6. This effect is largely negligible except for in very dense, massive clouds with low-temperature H II regions.

8 MODEL SET-UP

The parameter space invoked by the above set of equations is large. In this section we model a physically motivated subset of this parameter space to determine the importance of winds, radiation pressure and gravity in realistic conditions.

8.1 Criteria for complexity

We focus on four important criteria governing the state of the H II region:

(i) $C_{\rm w} > 1$, the condition for winds to become more important than photoionization in setting the expansion rate of the ionization front, given in equation (27),

(ii) $C_{\rm rp} > 1$, the condition for the perturbation from radiation pressure to exceed the thermal pressure from photoionization, given in equation (34),

(iii) $C_B > 1$, the condition that ionizing photons can break out of the shell around the H II region, given in equation (36), and

(iv) r_{launch} compared to the initial radius of the H II region, given in equation (37). This quantity is not scale-free and relies on gas dynamics and feedback physics on scales smaller than are studied in this paper.

In this section we calculate each criterion for a range of typical values in solar and sub-solar metallicity environments. A fully coupled time-dependent solution requires an iterative numerical solution and is beyond the scope of this paper. We instead suggest in which context simple H II region models considering only photoionization feedback may be employed, and offer scope for future model exploration.

8.2 Cloud properties

We focus on clouds with masses between 10^2 and 10^5 $M_\odot$ for individual stars and binaries, and up to 10^7 $M_\odot$ for clusters. Smaller clouds are unlikely to form massive stars. We expect larger clouds to follow the trends indicated at the higher end of our mass range.

We compute each condition for a range of surface densities from 10^2 to 10^4 $M_\odot$ pc^{-2}. The first value is typical of clouds in the solar neighbourhood (e.g. Lombardi et al. 2010), while the latter value is typical of clouds in the Galactic Central Molecular Zone (CMZ) (e.g. Walker et al. 2016). Note that the surface density threshold is also variable depending on which radius is selected, with higher densities closer to the peak of the density profile.

Where relevant, we assume that the cloud is not strongly accreting, i.e. $f = 1/2$ (see Appendix A). In the case of large accretion rates, $f \rightarrow 3/2$, and $n(r)$ would become a function of time.

We invoke two models for selecting our sources of radiation and winds from stars. In the first case we use a source that is an individual star, or two stars of the same mass (to approximate an equal-mass binary). We then give results for these individual stars from 5 to 120 $M_\odot$. The motivation here is to study how H II regions evolve around individual young massive stars or close binary systems.

In the second case, we use a source representing a cluster with an SFE of 10 per cent (i.e. the cluster mass is 10 per cent of the total gas mass inside r_0). To make this cluster, we draw randomly from a Chabrier (2003) initial mass function (IMF) up to the cluster mass. The cluster is created instantaneously, i.e. every star has the same age. This is designed to model young, compact clusters. In Section 10 we discuss how relevant this approximation is to observe structured giant molecular clouds.

8.3 Stellar evolution model

To calculate the quantities emitted by the stellar sources (e.g. wind momentum deposition rate, ionizing photon emission rate, ionizing photon energy), we use the stellar evolution model described in Geen et al. (2018), with a wind model based on Gatto et al. (2017). We use the rotating tracks given in the Geneva tables (Ekström et al. 2012), with spectra calculated in STARBURST99 (Leitherer et al. 2014) using these tracks. The surface temperature T_* for each star is taken from the Geneva tables and used to calculate the ionized gas temperature in Section 8.4.

We interpolate linearly between model tracks of different stellar masses. During the interpolation, each track is normalized to a time between 0 and 1, where 0 is the start of the zero age main sequence and 1 is the lifetime of the star. In this way, we optimize the ability for interpolated tracks to retain features in the neighbouring model tracks that scale with the lifetime of the stars. In Sections 9.2, 9.3, and 9.4, where not otherwise specified, we assume a stellar age of 1 Myr.

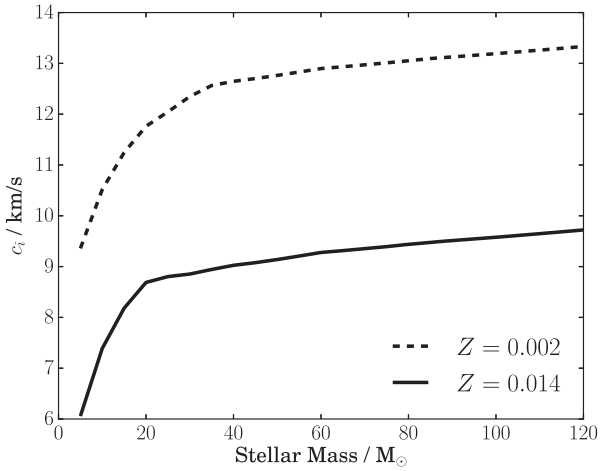

Figure 4. Ionized gas sound speed c_i in H II regions around each star of age 1 Myr with metallicities $Z = 0.002$ and $Z = 0.014$. See Section 8.4.

8.4 Ionized gas properties

In order to obtain reliable values for c_i, we use the spectral synthesis code CLOUDY (Ferland et al. 2017). We generate a table of ionized gas sound speeds c_i for a set of time-dependent stellar surface temperatures T_*, as well as gas density n_i, metallicity Z and ionization parameter $\mathcal{U}$. T_* is taken from the Geneva tables as described in Section 8.3. Where multiple stars are present (see Section 9.3), the temperature of the hottest star is used. To remove degeneracies in the solution, we pick a fiducial value of $n_i = 50$ cm^{-3} and $\mathcal{U} = -2$. Although n_i varies with time, it has a relatively weak effect on c_i. These values are plotted in Fig. 4.

To calculate α_B, we use the temperature-dependent model given in, e.g. appendix E2 of Rosdahl et al. (2013). The value in all cases is close to 2×10^{-13} cm^3 s^{-1}. We assume $\gamma = 4/3$.

9 RESULTS

In this section we present solutions to the models described in the previous sections. We begin by showing how the radius and density of an H II region in a specific environment evolves over time. We then calculate C_w, C_{rp}, C_B, and r_{launch} in a set of physically motivated conditions designed to explore where winds, radiation pressure, ionization front breakout, and gravity should become important. We solve these equations both for individual stars and for clusters sampled from an IMF. Model and parameter choices are given in Section 8. We focus for the majority of this section on solar metallicity results. In Section 9.4 we present results for low metallicity stars and clouds.

9.1 Evolution of an example H II region

Here we introduce an example H II region evolving under the influence of winds and UV photoionization. We pick a 120 $M_\odot$ star in a 10^4 $M_\odot$ cloud bounded by a surface density of 100 $M_\odot$ pc^{-2}. This is equivalent to the Orion A and B clouds, as listed in Lada, Lombardi & Alves (2010). However, this choice requires that these clouds have a single peaked density profile rather than multiple

density peaks, which is unrealistic. We choose this set of conditions largely to demonstrate a stronger response to winds and radiation pressure.

Fig. 5 shows the results of integrating the solutions to the equations in Sections 5 and 6, using the same parameters as introduced in these Sections (i.e. an efficiently cooling, momentum-driven wind, and radiation pressure terms where $f_{\rm trap} = 2$, $\phi_{\rm d} = 0.73$ and $\psi = 1$). We start from a radius of 0.001 pc and not 0 pc, since (a) in reality protostellar outflows set the initial radius of the H II region (see Kuiper & Hosokawa 2018), and (b) the ionization front cannot expand unless $r_{\rm i}$ is larger than the bistable point $r_{\rm launch}$.

The initial expansion of the H II region is faster in the case where winds are included, though at large radii there is little difference between the solutions. The wind bubble occupies most of the volume of the H II region at small radii, while at 20 pc the wind bubble radius $r_{\rm w}$ is only 20 per cent of the H II region radius $r_{\rm i}$.

The winds initially compress the H II region by a small factor, before causing its density to drop compared to a solution without winds. As with the radius, at later times the results with and without winds converge.

The contribution to the H II region's pressure from radiation pressure is between 16 and 18 per cent in this model. Photoionization is thus more important, but radiation pressure is significant enough to suggest that more detailed calculations with radiation pressure and winds included self-consistently should be considered for a complete model of the H II region. The small variations in $C_{\rm rp}$ in the bottom panel of Fig. 5 are due to changes in the surface temperature of the star, which in turn affects the equilibrium temperature of the photoionized gas.

When we include winds in the calculation, $C_{\rm rp}$ drops, i.e. winds reduce the impact of radiation pressure in this instance. This is due to the behaviour of equation (32), where $C_{\rm rp} \propto r_{\rm i}^{-2} n_{\rm i}^{-1}$. Radius $r_{\rm i}$ is larger at all times in the solution with winds (top panel in Fig. 5), and density $n_{\rm i}$ is initially larger (middle panel). This is because the wind bubble acts like a piston on the inside of the H II region, pushing and compressing it. Thus the overall effect of winds is to reduce $C_{\rm rp}$.

Having illustrated how one system behaves, we now explore how the effects of winds and radiation pressure change over a larger range of stellar and cloud parameters.

9.2 Single stars and pairs

In Fig. 6, we plot $C_{\rm w}$ and $C_{\rm rp}$ for H II regions of a given radius around single stars, with contours for pairs of equal-mass stars representing non-interacting binaries overlaid. These coefficients determine whether winds or radiation pressure significantly affect the dynamics of the H II region, respectively. Based on these results, winds and radiation pressure around single stars and binaries are most important at small radii, i.e. in the ultracompact H II region stage. The results for winds are consistent with the calculations of Capriotti & Kozminski (2001), who study a uniform external medium (i.e. $w = 0$, rather than $w = 2$ in this work). The use of equal-mass binaries gives winds a small boost, but radiation pressure a significantly larger boost. This is significant because, as Sana et al. (2012) argue, most massive stars are in binary pairs. As in Section 9.1, even when $C_{\rm rp}$ is less than 1, winds and radiation pressure combined have non-linear effects on the H II region and should be treated carefully.

Since we assume a quasi-hydrostatic internal structure for the H II region, $C_{\rm w}$ and $C_{\rm rp}$ are time-independent. However, the properties of the star(s) will affect the values obtained. We assume a

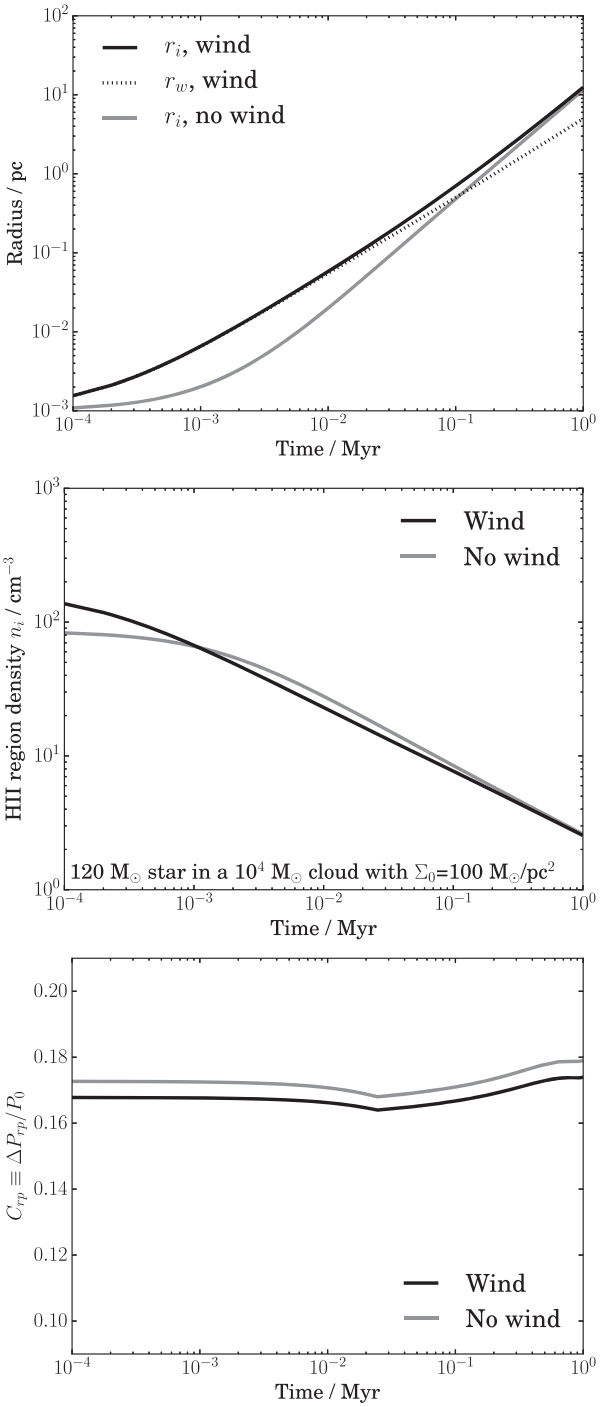

Figure 5. Plots showing the evolution of a single 120 $M_\odot$ star in a 10^4 $M_\odot$ cloud bounded by a surface density of 100 $M_\odot$ pc^{-2}. The top plot shows the evolution of the wind and ionization front radii $r_{\rm w}$ and $r_{\rm i}$ as given in equation (21). The middle plot shows the density of the H II region $n_{\rm i}$ in the same solution as given in equation (29) in solutions both including and ignoring stellar winds. The bottom plot shows the relative effect of radiation pressure and thermal pressure on the expansion of the H II region $C_{\rm rp}$ in equations (32) and (33). We start each solution at $r = 0.001$ pc since the photoionization-only equations have no defined solution if they start at $r = 0$.

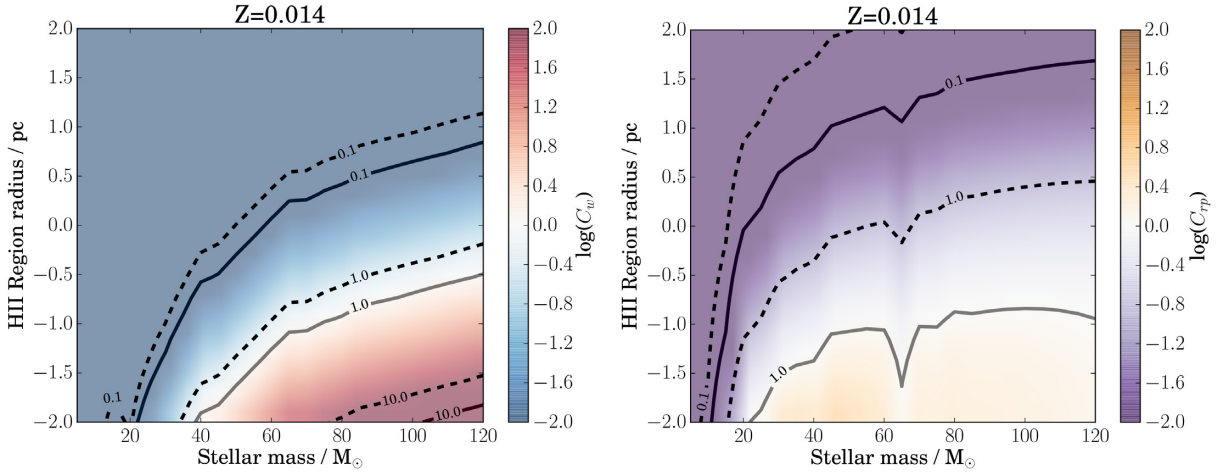

Figure 6. Surface plots of condition C_w for winds and $C_{\rm rp}$ for radiation pressure for H II regions of a given radius around single stars. A value of >1 means that winds or radiation pressure have a large influence on the dynamics of the H II region that cannot be ignored. Solid lines show results for a single star of a given mass and age 1 Myr on the x-axis, dashed lines for a pair of stars each with the given mass. The slight dip in $C_{\rm rp}$ at 65 $M_\odot$ is due to a change in the metal line absorption at this mass. The sound speed in the photoionized gas and other parameters used in these calculations discussed in Section 8.

young massive star of age 1 Myr, since we are principally interested in the early expansion of the H II region into the cloud. For very old clusters, the role of radiation (versus later kinetic processes such as supernovae) is reduced as the most massive stars die out. See Rahner et al. (2017) for a discussion of this phase and the relative importance of each feedback process.

In Fig. 7 we plot $C_{\rm w}$ and $C_{\rm rp}$ against cloud mass M_0 and bounding surface density Σ_0, where $r_{\rm i} = r_0$. Note for a given gas density field $n(r_i) \propto r_i^{-2}$, as $r_{\rm i}$ expands and encloses more mass, $M(<r_{\rm i})$ will increase and $\Sigma(r_{\rm i})$ will decrease. Winds are more important in very dense environments, either closer to the star or in globally denser clouds. Radiation pressure contributes at the 10 per cent level over a larger set of conditions, but rarely becomes more significant than photoionization except in dense environments or around equal-mass pairs of stars (again, this does not account for the role of interacting binaries in stellar evolution).

Fig. 8 shows the effect of gravity and addresses the question of whether the ionization front should be trapped by self-gravity of the cloud and/or accretion flows. Note that as in the previous Section, a *small* $r_{\rm launch}$ is required for the ionization front to escape in steeply peaked molecular clouds where $w > 3/2$. For stars above 20 $M_\odot$ in surface densities of $\Sigma_0 = 100$ $M_\odot$ pc^{-2}, $r_{\rm launch}$ is smaller than 0.1 pc, and so provided the ionization front can reach this point (via protostellar outflows, non-spherical geometries, or some other effect) it can readily accelerate outside the cloud. For very dense clouds, the ionization front needs to reach at least 0.1 pc for it not to be crushed by gravity. In this case, more details about the small-scale stellar and cloud physics that sets the initial H II region radius are needed to form a more concrete model for this phase.

Fig. 9 shows the condition for ionizing photons to break out of the D-type H II region and flood into the interstellar medium (ISM), i.e. $C_{\rm B} > 1$. This is possible for stars or binary pairs totalling above 70 $M_\odot$ in clouds bounded by $\Sigma_0 = 100$ $M_\odot$ pc^{-2}, assuming 10 per cent of the cloud mass is in stars. Since $C_{\rm B} \sim 1$ in this instance, the breakout is likely to be borderline rather than a strong divergence from the D-type solution. Once the breakout has occurred, the cloud is rapidly and fully ionized, and the density field expands at a few times the speed of sound in the ionized gas (Franco et al. 1990). For denser clouds, breakout is not possible. Note again that we do not discuss shell fragmentation here (see Rahner et al. 2019).

9.3 Small clusters

As the H II regions around individual stars merge, they form a larger H II region that expands through the cloud as a whole. In this Section we discuss models where this occurs. We assume, in the case where winds exist, that the wind bubbles merge. If they do not, then the effect of wind is significantly reduced. This case is discussed in some detail by Silich & Tenorio-Tagle (2017). It also assumes that winds cool efficiently, which we discuss in Section 5.

In Fig. 10 we invoke a cluster at $r = 0$ by randomly sampling from an IMF up to 10 per cent of the cloud mass (see Section 8.2). The cluster is assumed to be contained entirely within the H II region and wind bubble, i.e. the interaction between wind bubbles as in Silich & Tenorio-Tagle (2017) is ignored.

As in the single stellar case, winds only have an effect at the highest surface densities and cloud masses. Radiation pressure ($C_{\rm rp}$) is more dynamically important than winds ($C_{\rm w}$) in most cases, and can even reach the same importance as photoionization in certain conditions. Note, however, that this is not a full calculation of the role of radiation pressure, but an estimate of the perturbation that it gives to the solution. Where $C_{\rm rp}$ and $C_{\rm w}$ are large, future work should target these conditions with more realistic models. Full multiwavelength radiative hydrodynamic calculations including accurate dust models and cooling are needed to determine the precise role of radiation pressure and winds on H II regions.

Broadly, we expect photoionization to be the most significant driver of H II regions except in dense or high-mass clouds. In these clouds, more careful modelling is required, particularly since the SFE is likely larger than 10 per cent in these environments due to the relative inefficiency of feedback and short free-fall times (e.g. Vázquez-Semadeni et al. 2018; Rahner et al. 2019).

In Fig. 11 we plot $r_{\rm launch}$ and $C_{\rm B}$ for the same clusters. For small clusters, insufficient photons are available to either drive the H II region outwards or break out of the D-type solution. Between cloud masses of 10^3 and 10^4 $M_\odot$, the ability for an H II region to form (i.e. $r_{\rm launch}$ is small) depends on the sampling of the IMF. Above this mass, the ionization front is unlikely to stall.

For much larger clouds, photon breakout becomes likely. We caution again that very massive single power-law density profiles bounded by $\Sigma_0 = 100$ $M_\odot$ pc^{-2} are unlikely in conditions similar

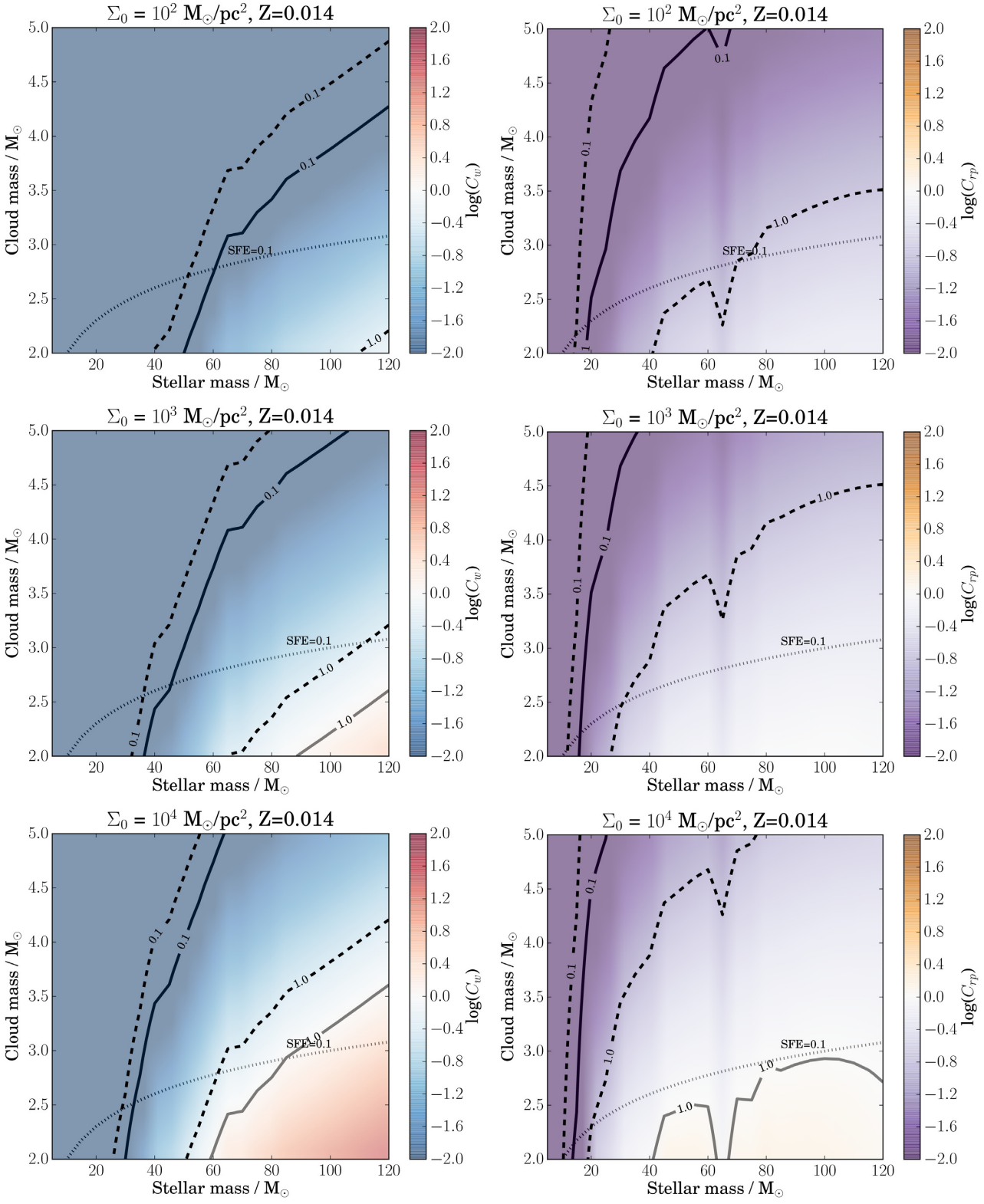

Figure 7. Surface plots of conditions $C_{\rm w}$ and $C_{\rm rp}$ at the cloud edge for single stars of age 1 Myr. A value >1 means that winds or radiation pressure exert more influence over the H II region than photoionization. Solid lines show results for a single star of a given mass on the *x*-axis, dashed lines for a pair of stars each with the given mass. Values are given at radius r_0 where the bounding surface density is Σ_0 and the initial enclosed mass is M_0 (see Section 3). A dotted line shows cloud masses 10× the star's mass to give an indication of where cloud masses at this ratio lie in the parameter space.

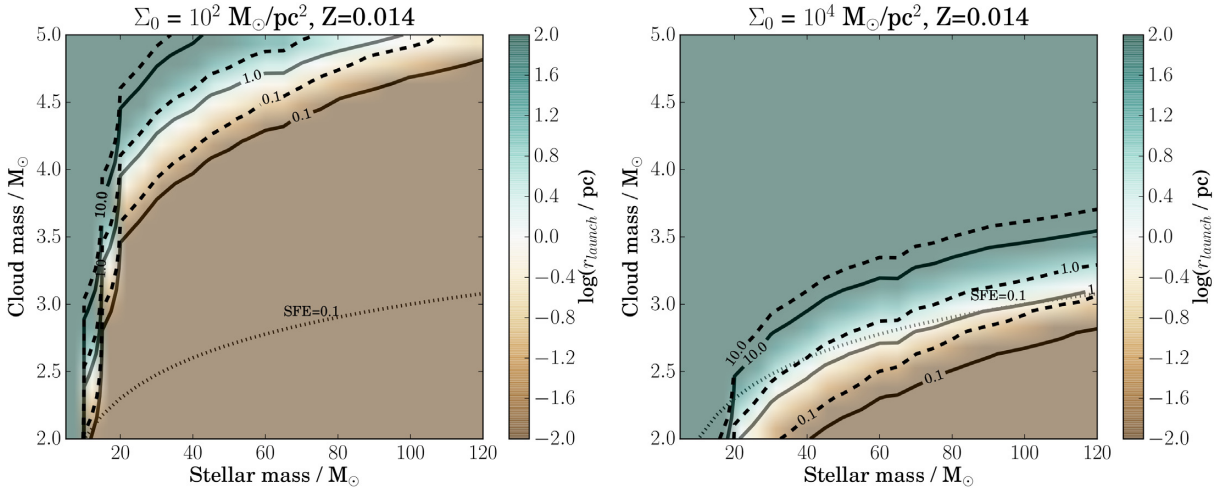

Figure 8. Surface plots of launch radius in pc for single stars of age 1 Myr at various cloud masses, enclosed by surface densities of 100 and 10 000 $M_\odot$ pc^{-2}, as in Fig. 7. Note that for steep density profiles, a *small* $r_{\rm launch}$ is required to allow the ionization front to expand. Solid lines show results for a single star of a given mass on the x-axis, dashed lines for a pair of stars each with the given mass. A dotted line shows cloud masses 10× the star's mass to give an indication of where cloud masses at this ratio lie in the parameter space.

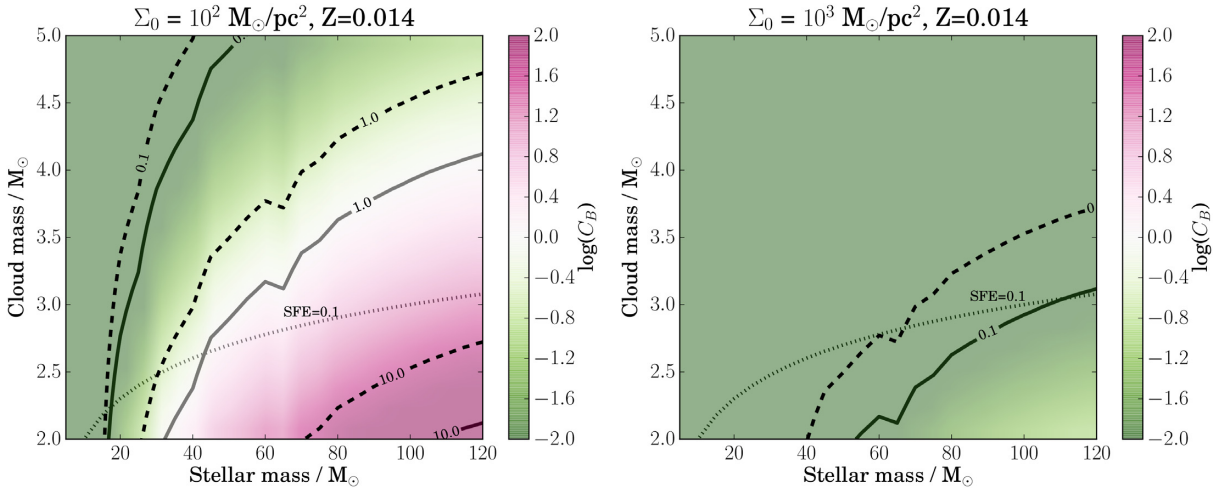

Figure 9. Surface plots of the breakout condition $C_{\rm B}$ for single stars of age 1 Myr at various cloud masses, enclosed by surface densities of 100 and 1000 $M_\odot$ pc^{-2}. $C_{\rm B} > 1$ implies that the ionization front should break out of its shell as calculated by Alvarez et al. (2006). Solid lines show results for a single star of a given mass on the x-axis, dashed lines for a pair of stars each with the given mass. A dotted line shows cloud masses 10× the star's mass.

to the solar neighbourhood. Observed systems with this mass and bounding density are likely structures made up of multiple peaked cores distributed in space.

9.4 Low-metallicity environments

In this section we modify the parameters used above to describe low metallicity environments. We make two changes. First, we use the low metallicity stellar tracks in the Geneva tables (Ekström et al. 2012), where $Z = 0.002$ (by comparison, solar metallicity is taken as $Z = 0.014$). Secondly, the equilibrium temperature of the ionized gas is higher due to less efficient metal line cooling (see Fig. 4).

In Fig. 12, we plot the criteria for winds and radiation pressure to be significant, $C_{\rm w}$ and $C_{\rm rp}$ by radius. Both parameters become smaller at low metallicity, i.e. winds and radiation pressure are less significant in these conditions. This is because firstly, winds are weaker in low metallicity stars, where the lower opacity in the stellar atmosphere reduces the ability for radiation inside the star to drive winds. Secondly, the steep dependence of the criteria on $c_{\rm i}$ means that increasing $c_{\rm i}$ drastically increases the efficiency of photoionization at driving the H II region.

In Fig. 13, we plot $r_{\rm launch}$ and $C_{\rm B}$ for low metallicity. Launching an accelerating H II region is even more likely than at solar metallicity. Breakout is however less likely. This is again because the increase in $c_{\rm i}$ greatly enhances the pressure inside the H II region.

10 DISCUSSION

In this Section we discuss the role of contexts outside the scope of this work on the evolution of the modelled H II regions.

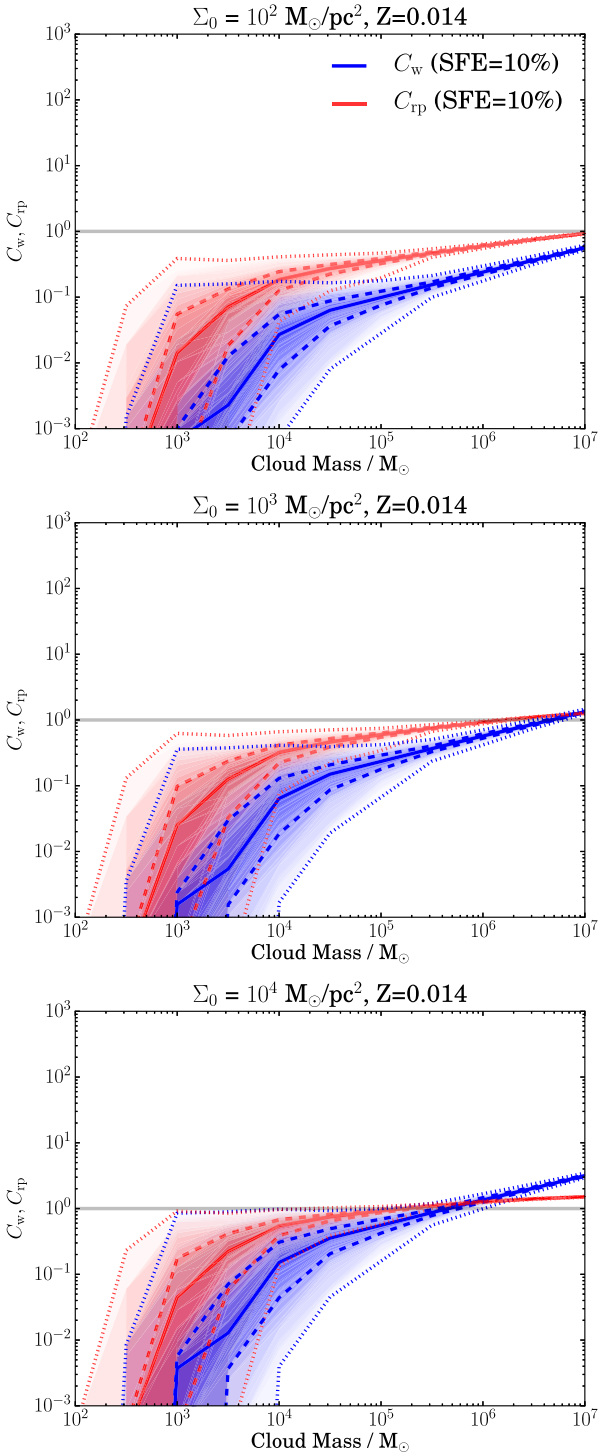

Figure 10. Surface plots showing conditions C_w and $C_{\rm rp}$ for clouds and clusters at various masses and surface densities, where values >1 indicate that the effect is more significant than the pressure from UV photoionization. The masses of stars in each cluster are randomly sampled from a Chabrier (2003) IMF up to a mass of 10 per cent of the cloud mass. $C_{\rm w}$ is shown in red and $C_{\rm rp}$ in blue. Dotted lines show the maximum and minimum values for each cluster mass, dashed lines show the interquartile range and solid lines the median. The shading shows everypercentile, where denser colour indicates a value closer to the median.

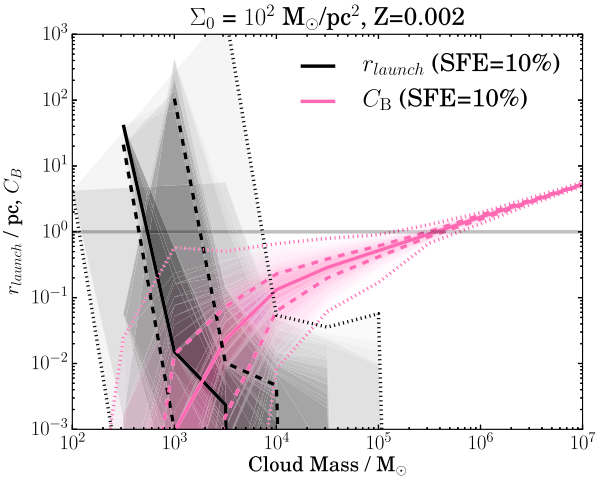

Figure 11. Surface plots showing $C_{\rm B}$ (the condition that ionizing photons break out of D-type front) and $r_{\rm launch}$ in pc for clouds and clusters at various masses and surface densities. Values are obtained as in Fig. 10. There is considerable scatter in the values for $r_{\rm launch}$, but the main limiting factor to launch an H II region is forming enough massive stars, which becomes ever more likely at higher cloud masses.

10.1 Conditions at small radii

Early in the star's lifetime, the system has $r_{\rm i} \rightarrow 0$. The physics of this phase is very important because, as we have established in this work, if the ionization front does not reach the bistable point at $r_{\rm launch}$, it cannot expand further.

The early phase of expansion of a photoionized H II region is modelled in 1D by Keto (2002), who determine stall conditions that allow continued accretion on to the protostar. Particularly important is the fact that at small radii, the force of gravity comes mainly from the star, not the gas, as is assumed here. This means that at low radii, where the cloud mass approaches the stellar mass, our results will become less realistic and alternative formulations should be used.

Simulations by Peters et al. (2011) demonstrate that disc dynamics, fragmentation and magnetohydrodynamics (MHD) play a strong role in the evolution of feedback bubbles close to the protostar, while Masson et al. (2016) and Vaytet et al. (2018) also demonstrate that non-ideal MHD is important at these scales. More recent simulation results by Kuiper & Hosokawa (2018), which include both winds and photoionization from an accreting protostar, argue that kinetic feedback from protostellar jets is the principal driver of the first bipolar outflows around a massive star, creating a channel for ionizing radiation and stellar winds to escape.

10.2 Conditions at large radii

Once the ionization front has left the cloud, the role of photoionization is diminished. As Haid et al. (2018) argue, the diffuse warm ISM is already ionized, so there is no further ionization front. Additionally, as the cloud is dispersed, the density drops, causing the cooling time of the winds to increase. Under these conditions, the role of winds will be enhanced, and more realistic numerical solutions for the cooling of the wind bubble are required. At late times, the most massive stars die, causing the ionizing photon emission rate to drop, and supernovae occur, leading to a supernova-driven structure (Rahner et al. 2017) that can, under certain conditions, recollapse and lead to a second star formation event (Rahner et al. 2018). A full picture of the interaction between

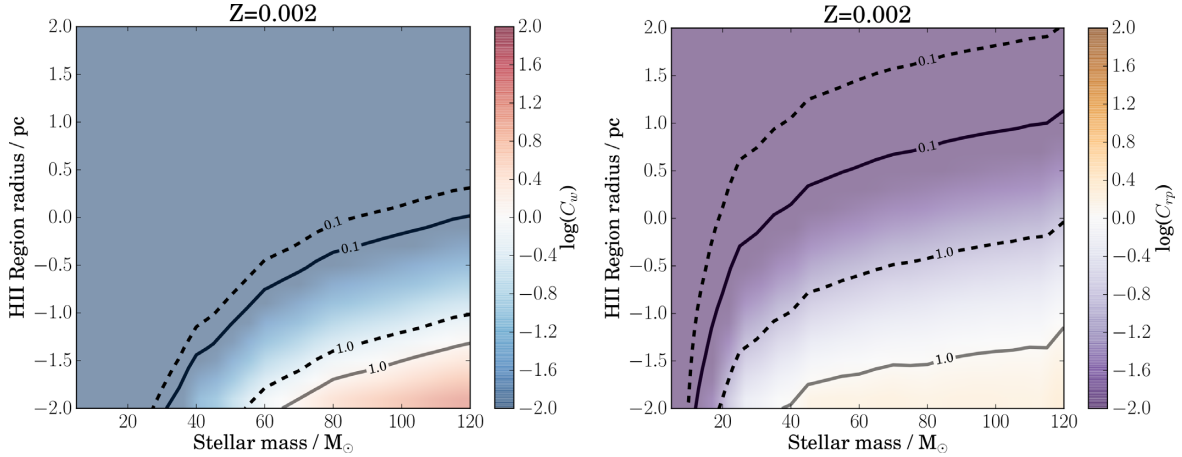

Figure 12. Surface plots of condition $C_{\rm w}$ for winds and $C_{\rm rp}$ for radiation pressure at various radii at low metallicity ($Z = 0.002$). See Fig. 6 for solar metallicity results.

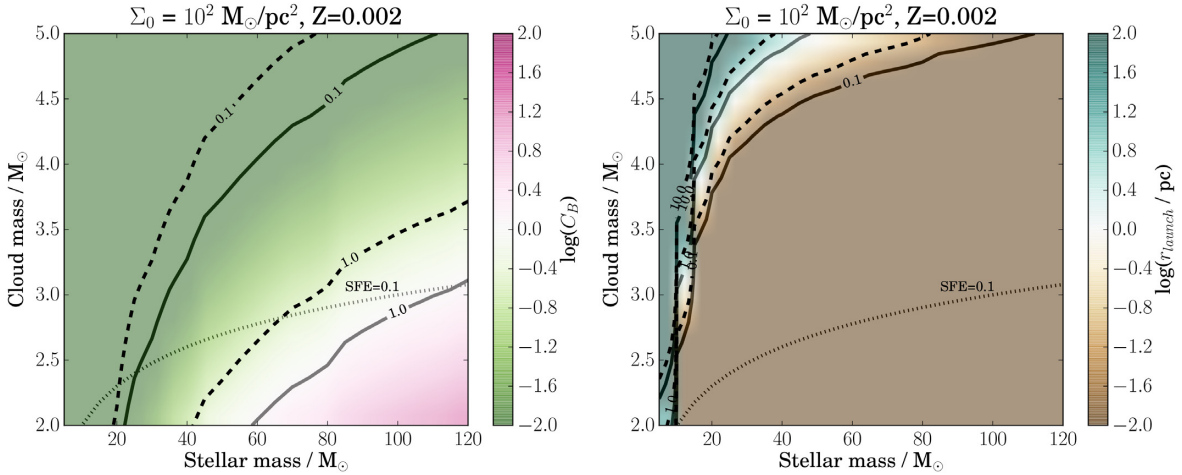

Figure 13. Surface plots of the breakout condition $C_{\rm B}$ (left) and the stall radius $r_{\rm stall}$ (right) for single stars and binaries at various cloud masses at low metallicity ($Z = 0.002$), enclosed by $\Sigma_0 = 100\ {\rm M}_\odot\ {\rm pc}^{-2}$. See Figs 8 and 9 for solar metallicity results.

stars and their surroundings is important for modelling the amount of momentum and radiation injected into the ISM of galaxies and how stars drive larger-scale flows.

The low metallicity results are important for understanding conditions at high redshift. They predict that, except in very dense conditions, photoionized H II regions should rapidly escape star-forming regions, dispersing clouds and creating flows of a few tens of $\rm km\,s^{-1}$. This suggests a high escape fraction from molecular clouds around the epoch of reionization, and provides a source of low-velocity turbulence in the galactic ISM.

10.3 The role of cloud structure

The models in this paper consider feedback in spherical gas clumps with $1/r^2$ density profiles. Molecular clouds observed in our Galaxy are argued to have fractal structures (e.g. Cartwright & Whitworth 2004), and so our analysis only applies provided that the density field around the star can be approximated by such a density profile. The interaction between multiple H II regions in neighbouring clumps, the ablation of clumps not containing massive stars by the H II region, changes in the density profile and other complicating effects are omitted from this work.

At some point, H II regions from neighbouring clumps will merge. As we discuss in Section 1.2, the embedded wind bubbles are not guaranteed to merge (Silich & Tenorio-Tagle 2017), which will reduce their efficiency, while leakage from porous shells further reduces their efficiency (Harper-Clark & Murray 2009). This will counter the effect in equation (26), where winds become more effective the more stars are emitting inside a single wind bubble and H II region.

10.4 Observational significance

The structure of H II regions affects their observable properties, since the density, temperature and radiation field determine the emission of radiation from the gas at each position inside the region. It is thus very important to understand the combined behaviour of photoionization, winds, and radiation pressure if we are to successfully interpret observed regions and understand the underlying physics of real systems. For example, models of photoionization-driven regions have recently been used to interpret the expansion of nearby H II regions in Tremblin et al. (2014) and Didelon et al. (2015). In particular, the latter paper makes it clear that the underlying assumptions about the region and its behaviour

strongly shape our interpretation of its current evolutionary state. If the expansion rate is faster than we predict, then we will overpredict the age of the source.

In Sections 5.4 and 5.5, we argue that even in cases where winds do not have a strong influence on the expansion of the H II region, a large wind bubble can exist. Such wind bubbles are observed in X-ray emission, since high gas temperatures are required to produce such photons, but they also affect the shape and structure of the H II region, which forms a shell between $r_{\rm w}$ and $r_{\rm i}$. We further note in Section 6.2 that if radiation pressure's influence is large enough, the combined effect of radiation pressure and winds on the photoionization solution becomes complex and can no longer be treated as a perturbation. Having identified likely regions of parameter space where this occurs, we must turn to more complete calculations to provide these solutions.

More complete analytic models of this nature have been used to target specific regions in Pellegrini et al. (2007, 2009). Draine (2011) focuses on parts of the parameter space where radiation pressure has a significant effect on the density structure of the photoionized gas, which in turn shapes the emission from the H II region. One quantity used to interpret such emission from H II regions is the ionization parameter, i.e. the ratio of ionizing photon to hydrogen density. This quantity has been calculated by Yeh & Matzner (2012) and Pellegrini et al. (2012) using full 1D hydrostatic analytic models including winds and radiation pressure. Emission from individual lines is also a useful tracer, and has been computed similarly in Yeh et al. (2013) and Verdolini et al. (2013). Such approaches are highly successful in reproducing emission line ratios from observed regions in nearby galaxies (Pellegrini et al. 2019). Complete radiative transfer models are also essential to obtain an accurate picture of the interaction between radiation at various energies and the gas inside H II regions.

11 CONCLUSIONS

In this paper, we (a) develop algebraic models to describe the expansion of photoionized H II regions under the influence of gravity and accretion in power-law density fields, (b) determine when terms describing winds, radiation pressure, gravity, and photon breakout become significant enough to affect the dynamics of the H II region, and (c) solve these expressions for a set of physically motivated conditions. We provide a set of expressions that can be used to calculate the dynamics and structure of observed H II regions, particularly the transition from thin shell H II regions to volume-filling H II regions and the role of radiation pressure in setting internal density gradients.

Photoionization heating is very efficient at driving an ionization front into cloud with steep power-law density fields (index $w > 3/2$). The time-scale for this expansion is set by the free-fall time in the cloud. In uniform density fields, ionization fronts tend towards a 'stall' radius where the expansion rate tends to zero. If $w > 3/2$, this is replaced with a 'launch' radius where the ionization front accelerates to infinity if the initial radius is larger than the launch radius.

We then focus on a singular isothermal sphere ($w = 2$) and introduce winds, radiation pressure, and photon breakout, as well as calculating the launch radius. As wind bubbles cool efficiently in dense cloud environments, both winds and radiation pressure are most important when the H II region radius is small ($\sim$0.1 pc radius). Their importance is enhanced at high surface densities. Under a larger range of conditions, their effect on the dynamics of the H II region is around 10 per cent of the contribution from photoionization, although radiation pressure can have a larger effect over a greater range. We caution that radiation pressure is a complex phenomenon. The radiation pressure parameters given in this paper are fiducial, but microphysics could decrease or even increase their values. The goal of this work is to provide estimates of which conditions it has a significant influence in, so that more detailed work can be carried out.

Both winds and radiation pressure shape the internal structure of the H II region even when they are not dynamically important, which has observational consequences. Conversely, a large wind bubble does not automatically mean that winds are dynamically important. However, winds, radiation pressure, and photoionization interact in non-linear ways, so even when winds or radiation pressure are not the most important process, care should be taken to consider their influence on the H II region once they approach non-negligible levels.

At solar metallicity, some photon breakout is possible for high mass stars in low density environments, while gravity prevents the expansion of H II regions only at very high densities. The calculations for photon breakout are lower limits, since this work omits shell fragmentation and non-spherical cloud geometries.

At low metallicity, photoionization becomes more efficient due to the higher equilibrium temperature of the photoionized gas. The role of winds, radiation pressure, photon breakout and gravity are all diminished. This has implications for galaxy formation simulations and theory, including the unresolved influence of photoionization-driven feedback and higher escape fractions than might be assumed when the structure of molecular clouds around young massive stars is unresolved.

The broad picture given by this paper is that H II regions around young massive stars are first driven by winds, radiation pressure or some other dynamical effect up 0.01–0.1 pc. Above this radius, photoionization accelerates the ionization front out of the cloud, where it enters the WIM or interacts with other dense clumps inside the star-forming region. This picture is complicated by the precise cooling rate of stellar winds, the detailed microphysics affecting radiation pressure inside H II regions, and conditions at high densities such as the Central Molecular Zone where gravity, winds, and radiation pressure compete with photoionization.

ACKNOWLEDGEMENTS

The authors would like to thank the referee for their careful and thoughtful comments in improving the paper. The authors would also like to thank Ashley Barnes, Simon Glover, Jo Puls, and Daniel Rahner for their useful comments and discussions during the preparation of this work. We acknowledge funding from the European Research Council under the European Community's Seventh Framework Programme (FP7/2007–2013). SG and RK have received funding from Grant Agreement no. 339177 (STARLIGHT) of this programme. EP and RK further acknowledge support from the Deutsche Forschungsgemeinschaft in the Collaborative Research Centre SFB 881 'The Milky Way System' (subprojects B1, B2, and B8) and in the Priority Program SPP 1573 'Physics of the Interstellar Medium' (grant numbers KL 1358/18.1, KL 1358/19.2). SG acknowledges support from a NOVA grant for the theory of massive star formation.

REFERENCES

Alvarez M. A., Bromm V., Shapiro P. R., 2006, ApJ, 639, 621
Avedisova V. S., 1972, SvA, 15, 708

Ballesteros-Paredes J., Klessen R. S., Mac Low M. M., Vazquez-Semadeni E., 2007, Protostars and Planets V. University of Arizona Press, Tucson, AZ USA, p. 63
Binney J., Tremaine S., 2008, Galactic Dynamics. 2nd edn., Princeton University Press, Princeton, NJ USA
Bisbas T. G. et al., 2015, MNRAS, 453, 1324
Capriotti E., Kozminski J., 2001, PASP, 113, 677
Cartwright A., Whitworth A. P., 2004, MNRAS, 348, 589
Castor J., Weaver R., McCray R., 1975, ApJ, 200, L107
Chabrier G., 2003, PASP, 115, 763
Dale J. E., 2015, Phys. Rev. B, 68, 1
Dale J. E., Ngoumou J., Ercolano B., Bonnell I. A., 2014, MNRAS, 442, 694
Davis S. W., Jiang Y.-F., Stone J. M., Murray N., 2014, ApJ, 796, 107
Didelon P., Motte F., Tremblin P., Hill T., 2015, A&A, 584, 25
Draine B. T., 2011, ApJ, 732, 100
Dunne B. C., Chu Y. H., Chen C. H. R., Lowry J. D., Townsley L., Gruendl R. A., Guerrero M. A., Rosado M., 2003, ApJ, 590, 306
Dyson J. E., 1977, A&A, 59, 161
Dyson J. E., Williams D. A., 1980, Physics of the Interstellar Medium. Halsted Press, New York
Ekström S. et al., 2012, A&A, 537, A146
Ferland G. J. et al., 2017, Rev. Mex. Astron. Astrofis., 53, 385
Fierlinger K. M., Burkert A., Ntormousi E., Fierlinger P., Schartmann M., Ballone A., Krause M. G. H., Diehl R., 2016, MNRAS, 456, 710
Forbes J. C., Krumholz M. R., Goldbaum N. J., Dekel A., 2016, Nature, 535, 523
Franco J., Tenorio-Tagle G., Bodenheimer P., 1989, Rev. Mex. Astron. Astrofis., 18, 65
Franco J., Tenorio-Tagle G., Bodenheimer P., 1990, ApJ, 349, 126
Gatto A. et al., 2017, MNRAS, 466, 1903
Geen S., Rosdahl J., Blaizot J., Devriendt J., Slyz A., 2015a, MNRAS, 448, 3248
Geen S., Hennebelle P., Tremblin P., Rosdahl J., 2015b, MNRAS, 454, 4484
Geen S., Hennebelle P., Tremblin P., Rosdahl J., 2016, MNRAS, 463, 3129
Geen S., Watson S. K., Rosdahl J., Bieri R., Klessen R. S., Hennebelle P., 2018, MNRAS, 481, 2548
Haid S., Walch S., Seifried D., Wünsch R., Dinnbier F., Naab T., 2018, MNRAS, 479, 4799
Harper-Clark E., Murray N., 2009, ApJ, 693, 1696
Haworth T. J., Harries T. J., Acreman D. M., Bisbas T. G., 2015, MNRAS, 453, 2278
Hennebelle P., Falgarone E., 2012, A&AR, 20, 55
Hosokawa T., Inutsuka S., 2006, ApJ, 646, 240
Jaffa S. E., Whitworth A. P., Clarke S. D., Howard A. D. P., 2018, MNRAS, 477, 1940
Kahn F. D., 1954, Bull. Astron. Inst. Neth., 12, 187
Kauffmann J., Pillai T., Shetty R., Myers P. C., Goodman A. A., 2010, ApJ, 716, 433
Keto E., 2002, ApJ, 580, 980
Keto E., 2007, ApJ, 666, 976
Kim J.-G., Kim W.-T., Ostriker E. C., 2016, ApJ, 819, 23
Kimm T., Blaizot J., Garel T., Michel-Dansac L., Katz H., Rosdahl J., Verhamme A., Haehnelt M., 2019, MNRAS, 486, 2215
Klessen R. S., Glover S. C. O., 2016, Star Formation in Galaxy Evolution, Saas-Fee Advanced Course, Vol. 43. Springer-Verlag Berlin Heidelberg, p. 85
Krumholz M. R., Matzner C. D., 2009, ApJ, 703, 1352
Krumholz M. R., Thompson T. A., 2012, ApJ, 760, 155
Krumholz M. R., Thompson T. A., 2013, MNRAS, 434, 2329
Kuiper R., Hosokawa T., 2018, A&A, 616, 22
Lada C. J., Lombardi M., Alves J. F., 2010, ApJ, 724, 687
Larson R. B., 1981, MNRAS, 194, 809
Lee Y.-N., Hennebelle P., 2018, A&A, 611, A88
Leitherer C., Ekström S., Meynet G., Schaerer D., Agienko K. B., Levesque E. M., 2014, ApJS, 212, 14
Li G.-X., Wyrowski F., Menten K., Megeath T., Shi X., 2015, A&A, 578, 15
Lombardi M., Alves J., Lada C. J., 2010, A&A, 519, 4
Mac Low M.-M., Klessen R. S., 2004, Rev. Mod. Phys., 76, 125
Mac Low M.-M., McCray R., 1988, ApJ, 324, 776
Masson J., Chabrier G., Hennebelle P., Vaytet N., Commerçon B., 2016, A&A, 587, 20
Mathews W. G., 1967, ApJ, 147, 965
Murray N., Quataert E., Thompson T. A., 2010, ApJ, 709, 191
Pellegrini E. W. et al., 2007, ApJ, 658, 1119
Pellegrini E. W., Baldwin J. A., Ferland G. J., Shaw G., Heathcote S., 2009, ApJ, 693, 285
Pellegrini E. W., Oey M. S., Winkler P. F., Points S. D., Smith R. C., Jaskot A. E., Zastrow J., 2012, ApJ, 755, 30
Pellegrini E. W., Rahner D., Reissl S., Glover S. C. O., Klessen R. S., Rousseau-Nepton L., Herrera-Camus R., 2019, preprint (arXiv:1909.09651)
Peters T., Banerjee R., Klessen R. S., Mac Low M.-M., 2011, ApJ, 729, 12
Raga A. C., Canto J., Rodriguez L. F., 2012, MNRAS, 419, L39
Rahner D., Pellegrini E. W., Glover S. C. O., Klessen R. S., 2017, MNRAS, 470, 4453
Rahner D., Pellegrini E. W., Glover S. C. O., Klessen R. S., 2018, MNRAS, 473, L11
Rahner D., Pellegrini E. W., Glover S. C. O., Klessen R. S., 2019, MNRAS, 483, 2547
Reissl S., Klessen R. S., Mac Low M.-M., Pellegrini E. W., 2018, A&A, 611, 19
Rosdahl J., Teyssier R., 2015, MNRAS, 449, 4380
Rosdahl J., Blaizot J., Aubert D., Stranex T., Teyssier R., 2013, MNRAS, 436, 2188
Sana H. et al., 2012, Science, 337, 444
Seon K.-I., Kwang-Il, 2009, ApJ, 703, 1159
Shapiro P. R., Iliev I. T., Alvarez M. A., Scannapieco E., 2006, ApJ, 648, 922
Shu F., Lizano S., Galli D., Canto J., Laughlin G., 2002, ApJ, 580, 969
Silich S., Tenorio-Tagle G., 2013, ApJ, 765, 10
Silich S., Tenorio-Tagle G., 2017, MNRAS, 465, 1375
Silich S., Tenorio-Tagle G., 2018, MNRAS, 478, 5112
Spitzer L., 1978, Physical Processes in the Interstellar Medium. Wiley-Interscience, New York
Strömgren B., 1939, ApJ, 89, 526
Tremblin P. et al., 2014, A&A, 568, A4
Vaytet N., Commerçon B., Masson J., González M., Chabrier G., 2018, A&A, 615, 18
Vázquez-Semadeni E., Zamora-Avilés M., Galván-Madrid R., Forbrich J., 2018, MNRAS, 479, 3254
Verdolini S. et al., 2013, ApJ, 769, 12
Vink J. S., Muijres L. E., Anthonisse B., de Koter A., Graefener G., Langer N., 2011, A&A, 531, 11
Walker D. L., Longmore S. N., Bastian N., Kruijssen J. M. D., Rathborne J. M., Galván-Madrid R., Liu H. B., 2016, MNRAS, 457, 4536
Weaver R., McCray R., Castor J., Shapiro P., Moore R., 1977, ApJ, 218, 377
Whitworth A., 1979, MNRAS, 186, 59
Yeh S. C. C., Matzner C. D., 2012, ApJ, 757, 18
Yeh S. C. C., Verdolini S., Krumholz M. R., Matzner C. D., Tielens A. G. G. M., 2013, ApJ, 769, 7

APPENDIX A: PRESSURE VELOCITIES IN AND ISOTHERMAL CLOUD

In this paper we define external forces on the shell in terms of velocity v_0, in order to provide a direct correction to the expansion velocity r_i.

We define v_0 as

$$v_0^2 = 2fGM(<r)r^{-1} = fv_{esc}^2, \quad \text{(A1)}$$

where $v_{\rm esc}$ is the escape velocity at r. f is a scaling factor that we determine below. For a cloud where $w = 2$, f is constant with respect to radius and of the order of unity except in the case where a central mass (i.e. the stellar source) exerts more gravitational force than the gas density $M(<r)$.

We assume in this paper that accretion on to the shell is modelled by a ram pressure, where the gas is at density ρ_0 and velocity $v_{\rm esc}$. This gives $f = 1$.

For gravitational acceleration, we take v_0 to be represented by the orbital velocity $\sqrt{GM(<r)r^{-1}}$. This gives $f = 1/2$. The combined f including both terms is thus 3/2.

Note that, as discussed in Section 3, we ignore the time evolution of ρ_0 due to accretion and the effect of the central mass of the star or cluster. This changes the form of equation (A1) and introduces radial dependencies to v_0. For examples of these calculations, see e.g. Keto (2002) and Didelon et al. (2015).

APPENDIX B: EXPANSION OF A PHOTOIONIZATION REGION WITH EXTERNAL PRESSURE

In Section 4 we give equation (11) to describe the expansion of an ionization front with an external pressure term, described as a velocity v_0 (see Appendix A).

We begin with equation (1) that describes the density profile in the neutral gas at r:

$$n(r) = n_0 (r/r_0)^{-w}, \tag{B1}$$

equation (9) that describes photoionization equilibrium inside the ionization front $r_{\rm i}$:

$$\frac{4\pi}{3} r_{\rm i}^3 n_{\rm i}^2 \alpha_{\rm B} = Q_{\rm H}, \tag{B2}$$

and equation (10) that describes pressure equilibrium at $r_{\rm i}$:

$$n_{\rm i} c_{\rm i}^2 = n(r_{\rm i})(\dot{r}_{\rm i} + v_0)^2. \tag{B3}$$

Equation (10) can be written in terms of density squared as

$$n_{\rm i}^2 c_{\rm i}^4 = n(r_{\rm i})^2 (\dot{r}_{\rm i} + v_0)^4 \tag{B4}$$

Substituting equation (9) for $n_{\rm i}$ and equation (1) for $n(r_{\rm i})$, this gives

$$c_{\rm i}^4 \frac{Q_{\rm H}}{\alpha_{\rm B}} \frac{3}{4\pi} = n_0^2 r_0^{2w} r_{\rm i}^{3-2w} (\dot{r}_{\rm i} + v_0)^4. \tag{B5}$$

When $r_{\rm i} = r_{\rm stall}$, $\dot{r}_i = 0$. We can thus divide the above equation by itself when these two terms are substituted:

$$1 = \left(\frac{r_{\rm i}}{r_{\rm stall}} \right)^{3-2w} \left(\frac{\dot{r}_{\rm i} + 1}{v_0} \right)^4. \tag{B6}$$

Hence if $R \equiv r_{\rm i}/r_{\rm stall}$, we recover equation (11). This gives us

$$r_{\rm stall}^{4w-7} = \left(\frac{3}{4\pi} \frac{Q_{\rm H}}{\alpha_{\rm B}} \right)^{-1} \left(8\pi f G \frac{m_{\rm H}}{X} \right)^2 \left(n_0 r_0^2 \frac{1}{c_{\rm i}} \right)^4 \tag{B7}$$

as in Geen et al. (2015b).

We can define a typical freefall time for the cloud

$$t_{\rm ff,0}^2 = \frac{3\pi}{32 G \rho_0} \tag{B8}$$

which using equations (3) and (A1) where $w = 2$ gives

$$v_0 = -\frac{r_0}{t_{\rm ff,0}} \frac{\pi}{2} \sqrt{3f} \tag{B9}$$

Substituting for v_0 using equation (B9) and taking $w = 2$ gives

$$\dot{R} = R_0 \frac{\pi}{2} \frac{\sqrt{3f}}{t_{\rm ff,0}} (R^{1/4} - 1), \tag{B10}$$

where $R_0 \equiv r_0/r_{\rm stall}$. As stated previously in the paper, for $w > 3/2$, $r_{\rm stall}$ becomes a 'launching' radius $r_{\rm launch}$ that the solutions accelerate away from rather than converging to.

APPENDIX C: WIND AND PHOTOIONIZATION DYNAMICAL EQUATIONS

In this section we derive equation (21) that describes the dynamical evolution of an ionization front with an embedded wind source.

The solution is similar to that in equation (B). We amend equation (9) to include a collisionally ionized sphere up to r_w:

$$\frac{4\pi}{3} (r_{\rm i} - r_{\rm w})^3 n_{\rm i}^2 \alpha_{\rm B} = Q_{\rm H}. \tag{C1}$$

In addition, we have equation (20) that describes the pressure balance at $r_{\rm w}$ from a momentum-conserving wind:

$$\frac{\dot{p}_{\rm w}}{4\pi r_{\rm w}^2} = n_{\rm i} c_{\rm i}^2 \frac{m_{\rm H}}{X}. \tag{C2}$$

We begin by substituting $r_{\rm w}$ in equation (C1) with equation (C2):

$$r_{\rm i}^3 - \left(\frac{\dot{p}_{\rm w}}{4\pi} c_{\rm i}^2 \frac{X}{m_{\rm H}} \frac{1}{n_{\rm i}} \right)^{3/2} = \frac{Q_{\rm H}}{\alpha_{\rm B}} \frac{3}{4\pi} \frac{1}{n_{\rm i}^2}. \tag{C3}$$

We then substitute $n_{\rm i}$ in this equation for equation (10)

$$r_{\rm i}^3 - \left(\frac{\dot{p}_{\rm w}}{4\pi} \frac{X}{m_{\rm H}} \right)^{3/2} \left(\frac{n_0 r_0^2 (\dot{r}_{\rm i} + v_0)^2}{r_{\rm i}^2} \right)^{-3/2} = \frac{Q_{\rm H}}{\alpha_{\rm B}} \frac{3}{4\pi} \left(\frac{1}{c_{\rm i}^2} \frac{n_0 r_0^2 (\dot{r}_{\rm i} + v_0)^2}{r_{\rm i}^2} \right)^{-2}. \tag{C4}$$

Multiplying and dividing by terms in $r_{\rm i}$ and $\dot{r}_{\rm i} + v_0$) we obtain

$$(\dot{r}_{\rm i} + v_0)^4 = \left(\frac{\dot{p}_{\rm w}}{4\pi} \frac{X}{m_{\rm H}} \frac{1}{n_0 r_0^2} \right)^{3/2} (\dot{r}_{\rm i} + v_0) + \frac{Q_{\rm H}}{\alpha_{\rm B}} \frac{3}{4\pi} \left(\frac{c_{\rm i}^2}{n_0 r_0^2} \right)^2 r_{\rm i} \tag{C5}$$

which gives us equation (21) and terms for A_w and $A_{\rm i}$ as defined there.

APPENDIX D: THE ROLE OF GRAVITY IN THE H II REGION

In addition to radiation pressure, self-gravity can also set up a gradient inside the H II region. We assume here that the H II region has a uniform density $n_{\rm i}$ and calculate the conditions where the pressure from gravity should set up a gradient.

The pressure from self-gravity acting on a spherical shell of thickness dr at radius r, where $r < r_{\rm i}$ is

$$\mathrm{d}P_{\rm g} = -\frac{G M_{\rm i}(<r)\,\mathrm{d}m}{r^2} \frac{1}{4\pi r^2}, \tag{D1}$$

where $M_{\rm i}(<r)$ is the mass in ionized gas contained within r, or $\frac{4}{3}\pi r^3 n_{\rm i} \frac{m_{\rm H}}{X}$, the mass of the spherical shell $\mathrm{d}m = \frac{m_{\rm H}}{X} n_{\rm i} 4\pi r^2\,\mathrm{d}r$. This

gives

$$\mathrm{d}P_{\mathrm{g}} = -4\pi G n_{\mathrm{i}}^2 \left(\frac{m_{\mathrm{H}}}{X}\right)^2 \frac{r}{3}\,\mathrm{d}r. \tag{D2}$$

Equating this to the thermal pressure of the photoionized gas at r and integrating the result, we obtain

$$\frac{n_{\mathrm{inner}}}{n_{\mathrm{outer}}} = C_{\mathrm{g}} + 1, \tag{D3}$$

where

$$C_{\mathrm{g}} \equiv \frac{\pi G r^2 m_{\mathrm{H}}}{6 c_{\mathrm{i}}^2 X} n_{\mathrm{inner}}. \tag{D4}$$

Note that the condition $C_{\mathrm{g}} \ll 1$ defines whether or not the gradient due to gravity is important, since these solutions assume that $n_{\mathrm{inner}} \simeq n_{\mathrm{outer}}$. In equation (17) we argue that $n_{\mathrm{i}}/n(r) \simeq 0.1$–1. We can thus substitute for $n_{\mathrm{i}} r^2 \simeq n(r) r^2 = n_0 r_0^2$. Substituting this with equations (7) and (8), we can write

$$C_{\mathrm{g}} = 6.37 \times 10^{-4} \left(\frac{c_{\mathrm{i}}}{10\,\mathrm{km\,s^{-1}}}\right)^{-2} \left(\frac{M_0}{100\,\mathrm{M_\odot}}\right)^{1/2} \times \left(\frac{\Sigma_0}{100\,\mathrm{M_\odot\,pc^{-2}}}\right)^{1/2}. \tag{D5}$$

Since this is an upper bound, and requires very dense clouds with low-temperature photoionization regions, we neglect the effect of self-gravity inside the H II region in this work.

This paper has been typeset from a TEX/LATEX file prepared by the author.